



Original Article

# Artesunate Induces Ferroptosis in Hepatic Stellate Cells and Alleviates Liver Fibrosis via the ROCK1/ATF3 Axis

Yingqian Wang<sup>1</sup>, Yujia Li<sup>1</sup>, Yangling Qiu<sup>1</sup>, Min Shen<sup>2</sup>, Ling Wang<sup>1</sup>, Jiangjuan Shao<sup>1</sup>, Feng Zhang<sup>1,3</sup>, Xuefen Xu<sup>1</sup>, Zili Zhang<sup>1,3\*</sup>, Mei Guo<sup>1\*</sup> and Shizhong Zheng<sup>1,3\*</sup>

<sup>1</sup>Jiangsu Key Laboratory for Pharmacology and Safety Evaluation of Chinese Materia Medica, Nanjing University of Chinese Medicine, Nanjing, Jiangsu, China; <sup>2</sup>Institute of Translational Medicine, Medical College, Yangzhou University, Yangzhou, Jiangsu, China; <sup>3</sup>Jiangsu Key Laboratory of Therapeutic Material of Chinese Medicine, Nanjing University of Chinese Medicine, Nanjing, Jiangsu China

Received: 9 April 2023 | Revised: 7 July 2023 | Accepted: 19 July 2023 | Published online: 25 August 2023

## Abstract

**Background and Aims:** Development of fibrosis in chronic liver disease requires activation of hepatic stellate cells (HSCs) and leads to a poor outcome. Artesunate (Art) is an ester derivative of artemisinin that can induce ferroptosis in HSCs, and activated transcriptional factor 3 (ATF3) is an ATF/CREB transcription factor that is induced in response to stress. In this study, we examined the role of the Rho-associated protein kinase 1 (ROCK1)/ATF3 axis in Art-induced ferroptosis in HSCs. **Methods:** HSC activation and ferroptosis were studied *in vitro* by western blotting, polymerase chain reaction, immunofluorescence, and other assays. ATF3 electrophoretic mobility and ROCK1 protein stability were assayed by western blotting. Immunoprecipitation was used to detect the interaction of ROCK1 and ATF3, as well as ATF3 phosphorylation. A ubiquitination assay was used to verify ROCK1 degradation. Atf3-interfering and Rock1-overexpressing mice were constructed to validate the anti-hepatic fibrosis activity of Art *in vivo*. **Results:** Art induced ferroptosis in HSCs following glutathione-dependent antioxidant system inactivation resulting from nuclear accumulation of unphosphorylated ATF3 mediated by ROCK1-ubiquitination

*in vitro*. Art also decreased carbon tetrachloride-induced liver fibrosis in mice, which was reversed by interfering with Atf3 or overexpressing Rock1. **Conclusions:** The ROCK1/ATF3 axis was involved in liver fibrosis and regulation of ferroptosis, which provides an experimental basis for further study of Art for the treatment of liver fibrosis.

**Citation of this article:** Wang Y, Li Y, Qiu Y, Shen M, Wang L, Shao J, *et al.* Artesunate Induces Ferroptosis in Hepatic Stellate Cells and Alleviates Liver Fibrosis via the ROCK1/ATF3 Axis. *J Clin Transl Hepatol* 2024;12(1):36–51. doi: 10.14218/JCTH.2023.00162.

## Introduction

Liver fibrosis develops during the progression of chronic liver disease (e.g., viral hepatitis, alcoholic and nonalcoholic fatty liver disease) to cirrhosis, hepatic failure, or hepatocellular carcinoma, and is caused by hepatic damage repair decompensation.<sup>1</sup> Inflammatory factors released by hepatic parenchymal and nonparenchymal cells activate HSCs during persistent liver injury. Following activation, hepatic stellate cell (HSC) proliferation increases and they secrete extracellular matrix (ECM) to drive the fibrotic process. Scavenging activated HSCs has been reported to decrease fibrosis.<sup>2</sup> Our study aimed to identify effective methods of removing activated HSCs.

Ferroptosis is a form of programmed cell death that differs from pyroptosis, apoptosis, and necroptosis. It is distinguished by glutathione (GSH) depletion, intracellular iron accumulation, and generation of lipid peroxidation products.<sup>3</sup> Targeting ferroptosis of HSCs may become a way to treat liver fibrosis.<sup>4</sup> Glutathione peroxidase 4 (GPX4) and solute carrier family 7, member 11 (SLC7A11) are antioxidants and their deficiency results in ferroptosis. GSH scavenges excess reactive oxygen species (ROS) produced during cell damage.<sup>5</sup> Studies have shown that ferroptosis is regulated by transcription factors (TFs), such as nuclear factor erythroid 2-related factor 2 (NRF2), activating transcription factor 4 (ATF4) and p53.<sup>6–8</sup> TFs recognize and bind to specific sequences within ferroptosis-related genes, recruit coactivators, assemble to form preinitiation complexes, and promote

**Keywords:** Ferroptosis; Liver fibrosis; Antioxidant system; ATF3; ROCK1.

**Abbreviations:**  $\alpha$ -SMA, alpha-smooth muscle actin; ALP, alkaline phosphatase; ALT, alanine aminotransferase; AP-1, activator protein 1; ARE, antioxidant response element; Art, artesunate; ART, artemether; AST, aspartate aminotransferase; ATF3, activated transcriptional factor 3; ATF4, activating transcription factor 4; CCl<sub>4</sub>, carbon tetrachloride; CHX, cycloheximide; DHA, dihydroartemisinin; DMSO, dimethyl sulfoxide; DMEM, Dulbecco's modified essential medium; ECM, extracellular matrix; EGFR, epidermal growth factor receptor; FBS, fetal bovine serum; Fer-1, ferrostatin-1; GAPDH, glyceraldehyde phosphate dehydrogenase; GSH, glutathione; HA, hyaluronic acid; HSC, hepatic stellate cell; IV-C, IV collagen; LN, laminin; LO2, human hepatocyte; LX2, human activated hepatic stellate cell; MDA, malondialdehyde; NOX4, NADPH oxidase 4; NRF2, nuclear factor erythroid 2-related factor 2; PBS, phosphate-buffered saline; PC-III, procollagen type III; PDGFR $\beta$ , platelet-derived growth factor receptor  $\beta$ ; POR, NADPH-cytochrome P450 reductase; RhoA, Ras homolog gene family member A; ROCKs, Rho-associated coiled-coil containing protein kinases; ROCK1, Rho-associated protein kinase 1; ROS, reactive oxygen species; siRNA, short interfering RNA; SLC7A11, solute carrier family 7, member 11; TEM, transmission electron microscopy; TF, transcription factor.

\*Correspondence to: Shizhong Zheng, Mei Guo and Zili Zhang, Nanjing University of Chinese Medicine, 138 Xianlin Avenue, Nanjing, Jiangsu 210023, China. ORCID: <https://orcid.org/0000-0003-4925-9390> (SZ), <https://orcid.org/0009-0005-9861-926X> (MG) and <https://orcid.org/0000-0001-6506-648X> (ZZ). Tel/Fax: +86-25-85811246, E-mail: nytws@njucm.edu.cn (SZ), 3701110@njucm.edu.cn (MG), zilizhang@njucm.edu.cn (ZZ).

transcription or repression via RNA polymerase II.<sup>9,10</sup> Nevertheless, more investigation is required to understand how TFs regulate the antioxidant system in ferroptosis.

Activated transcriptional factor 3 (ATF3) is a member of the ATF/CREB family, which is involved in the transcriptional regulation of cellular life activity. ATF3 is an adaptive response gene that enables cells to swiftly react to changes in the environment.<sup>11</sup> ATF3 identifies and combines with consensus sequences on the antioxidant response element (ARE) including TGACGTCA to regulate target genes, [e.g., SLC7A11 and NADPH oxidase 4 (NOX4)], involved in regulating oxidative stress.<sup>12,13</sup> Indeed, ATF3 is closely associated with multiple organic fibrosis and hepatic steatosis. Effective prevention of cardiac hypertrophy and fibrosis is achieved by overexpression of ATF3 in cardiac fibroblasts.<sup>14</sup> ATF3 upregulates IncIAPF transcription to accelerate the deterioration of pulmonary fibrosis.<sup>15</sup> Moreover, hepatocyte-specific ATF3 overexpression accelerates triglyceride hydrolysis and delays the development of nonalcoholic fatty liver disease/nonalcoholic steatohepatitis.<sup>16</sup> Rho-associated coiled-coil containing protein kinases (ROCKs) are essential downstream target genes of the Ras homolog gene family, member A (RhoA) and are responsible for phosphorylating target proteins to regulate cytoskeleton formation, cell proliferation and migration, and cell death. For example, the ROCK1/PTEN/PI3K signaling pathway regulates cofilin phosphorylation, mitochondrial translocation, and death of malignant cells.<sup>17</sup> ROCK1 controls sepsis-induced acute kidney damage through TLR2-mediated pyroptosis.<sup>18</sup> CircCUL2 promotes autophagy and inhibits the malignant growth of gastric cancer cells by regulating miR-142-3p/ROCK2.<sup>19</sup> ROCK1 and ROCK2 are two isoforms of this family and the former is more abundant in liver tissue.<sup>20</sup> Studies have shown that inhibition of ROCKs regulates the phosphorylation of ATF3 and its nuclear entry.<sup>21</sup> However, whether ROCKs directly interacts with ATF3 and their role in liver fibrosis needs further study.

Currently, natural medicines for liver fibrosis treatment have received widespread attention. Artemisinin is a natural antimalarial compound extracted from the plant *Artemisia annua* Linn. Art is a succinic acid half ester derivative of artemisinin with increased antimalarial potency.<sup>22</sup> Studies have shown that the inhibitory effectiveness of Art on liver fibrosis results in part from ferritinophagy of activated HSCs, but the mechanism remains to be revealed.<sup>23</sup> This study investigated whether Art regulates ATF3 and inhibits GSH-dependent antioxidant activity to induce ferroptosis in HSCs and decrease fibrosis.

## Methods

### Animal experiments

The Institutional Animal Care and Use Committee of Nanjing University of Chinese Medicine approved the animal protocols. All animals were treated humanely following National Institutes of Health guidelines. Sixty 8-week-old 18–22 g male ICR mice were purchased from Hangzhou Medical College (production license SCXK Zhejiang 2019-0002). The mice were bred and maintained under specific-pathogen free conditions. Mice were given an intraperitoneal injection of CCl<sub>4</sub> in olive oil (1:9 v/v) to cause liver fibrosis<sup>24</sup> and divided into ten groups for treatment with vehicle, CCl<sub>4</sub>, CCl<sub>4</sub>+Art (5 mg/kg), CCl<sub>4</sub>+Art (10 mg/kg), CCl<sub>4</sub>+Art (20 mg/kg), CCl<sub>4</sub>+colchicine (0.1 mg/kg), CCl<sub>4</sub>+VA-Lip-Atf3-shRNA, CCl<sub>4</sub>+VA-Lip-Atf3-shRNA+Art (10 mg/kg), CCl<sub>4</sub>+VA-Lip-Rock1-plasmid, CCl<sub>4</sub>+VA-Lip-Rock1-plasmid+Art (10 mg/kg). After the first week, mice were injected intraperito-

neally with 10% CCl<sub>4</sub> three times a week. An Atf3-shRNA and Rock1-plasmid was injected into the caudal vein once every 2 weeks, twice in total. Throughout the course of 5–8 weeks, Art (0, 5, 10, or 20 mg/kg) was dissolved in olive oil, colchicine (0.1 mg/kg) was dissolved in saline and injected intraperitoneally once daily. Control vector (VA-Lip-control-vector), Atf3 shRNA (VA-Lip-Atf3-shRNA), and Rock1 plasmid (VA-Lip-Rock1-plasmid) were constructed and injected into the caudal vein. Details of the animal procedures are shown in Supplementary Fig. 1. Blood and liver samples were collected at the end of the study.

### Histological analysis

Fresh liver tissue was immersed 4% paraformaldehyde for 12 to 24 h, dehydrated in an ethanol series, cleared in xylene, embedded in paraffin, and sectioned. Liver sections were stained with hematoxylin and eosin, Masson stain, and sirius red. Immunohistochemical staining of fibrosis indicators was done as previously reported.<sup>25</sup> Immunofluorescence and Prussian blue staining were performed by Servicebio (Wuhan, China).

### Chemicals and antibodies

Artesunate (Art, K913007-5 g) and colchicine (Q107209-250 mg) were purchased from ShangHai D&B Biological Science and Technology (Shanghai, China). Carbon tetrachloride (CCl<sub>4</sub>; 488488) and dimethyl sulfoxide (DMSO; D2650) were acquired from Sigma Aldrich (St Louis, MO, USA). Trypsin-EDTA (25200056), fetal bovine serum (FBS; 10099-141), phosphate-buffered saline (PBS; 10010023), Opti MEM medium, and Dulbecco's modified essential medium (DMEM; 12491) were obtained from GIBCO BRL (Grand Island, NY, USA).

Primary antibodies against epidermal growth factor receptor (EGFR; 2085S) and platelet-derived growth factor receptor  $\beta$  (PDGFR $\beta$ ; 3169) were provided by Cell Signaling Technology (Danvers, MA, USA). Anti-rabbit IgG (ab150077) and anti-mouse IgG (ab6728) were bought from Abcam (Cambridge, UK). Primary antibodies against alpha-smooth muscle actin ( $\alpha$ -SMA; ab124964), Collagen I (ab138492), Fibronectin (ab45688), ATF3 (ab207434), ROCK1 (ab134181) and ROCK2 (ab125025) were obtained from Abcam. We purchased ROCK1 (21850-1-AP) from Proteintech (Rosemont, IL, USA).  $\beta$ -actin rabbit pAb (AC006), ubiquitin rabbit pAb (A18185) from ABclonal Technology (Woburn, MA, USA). Anti PHOSPHO-SER/THR-PRO MPM-2 (05-368) was bought from Millipore (Burlington, MA, USA). Ferrostain-1 (Fer-1) (HY-100579), MG-132 (HY-13259), cycloheximide (CHX; HY-12320), NAC (HY-134495) and CQ (HY-17589A) were bought from MedChemExpress (Monmouth, NJ, USA).

### Plasmid construction

Short interfering RNA (siRNA) targeting ATF3 and nontarget siRNA control vector were constructed by Yorbio Tech (Nanjing, China), and the sequences are listed in Table 1. pcDNA3.1-ROCK1, pcDNA3.1-ATF3, and control vector were obtained from Yorbio Tech. Western blotting was performed to analyze transfection efficiency. VA-Lip-Control-vector, VA-Lip-Atf3-shRNA, and VA-Lip-Rock1-plasmid were prepared as previously described.<sup>26</sup>

### Construction of ATF3 mutant plasmids

A threonine phosphorylation site mutation was constructed by PCR-mediated mutagenesis as previously described.<sup>27</sup> Briefly, the primer pairs forward 5'- GCTAGTTAAGCTTGGTACCGAGCTCGGATCCGCCACCATGATGCTCAAC-3' and re-

**Table 1. ATF3 siRNA sequences used for transfection**

hATF3 si-1	Sense	5'-GAUGAGAGAAACCUCUUUATT-3'
	Antisense	5'-UAAAGAGGUUUCUCUCAUUCTT-3'
hATF3 si-2	Sense	5'-AUGUCCUCUGCGCUGGAAUUT-3'
	Antisense	5'-AUUCCAGCGCAGAGGACAUTT-3'
hATF3 si-3	Sense	5'-UCACAAAAGCCGAGGUAGCTT-3'
	Antisense	5'-GCUACCUCGGCUUUUGUGATT-3'

ATF3, activated transcriptional factor 3.

verse 5'-CTTTGTAGTCGAAGGGCCCTCTAGACTCGAGGCTCTG-CAATGTTTC-3' were used to construct the ATF3-WT plasmid and 5'-CTTCTGGATCCCTCCATTCTGAGCCCGGAC-3' and 5'-GAATGGGAGGGATCCAGAAGATGAGAGAAACC-3' were used to construct the ATF3 phosphorylation site mutation plasmid (ATF3-Mut). ATF3-WT and ATF3-Mut were confirmed by Sanger sequencing by WZ Bioscience (Shandong, China).

#### Cell culture and transfection

The HSC-LX2 (BNCC337957) immortal human HSC line was obtained from the BeNa culture collection (Beijing, China). LO2 human normal hepatocytes were obtained from the Chinese Academy of Sciences Cell Bank (Shanghai, China). Cells were grown in DMEM supplemented with 10% FBS and 1% antibiotics at 37°C with 5% CO<sub>2</sub>. pcDNA3.1-ROCK1, pcDNA3.1-ATF3 plasmids and control vector were transfected into the HSCs with HiFectPlus (Hifect-H-001) from ICRe Bioscience Technology (Nanjing, China) according to the manufacturer's instructions.

#### Western blotting

RIPA lysate was used for cellular protein extraction. Cells were homogenized after adding RIPA, phosphatase inhibitor and protease in a ratio of 100:1:1. A nano drop assay was used to measure protein concentration, 5× loading buffer (P0015L; Beyotime, Shanghai, China) was added to each sample and heated in a water bath for 15 m. Proteins were separated by molecular weight with sodium dodecyl sulfate polyacrylamide gel electrophoresis and subsequently transferred to polyvinylidene difluoride membranes. After blocking, with 5% skim milk at room temperature for 2 h, the im-

munoblots were incubated with the target primary antibodies overnight at 4°C, washed three times in 1× tris-buffered saline with 0.1% Tween 20 before being incubated with the secondary antibody for 2 h at room temperature. Following the incubation, autoradiography was carried out. ATF3 electrophoretic mobility was determined as previous reported.<sup>28</sup>

#### RNA extraction and real-time polymerase chain reaction (RT-PCR)

Following the manufacturer's instructions, Trizol reagent (15596018; Invitrogen, Waltham, MA, USA) was used to extract RNA from LX2 cells and reverse transcribed to cDNA which stored at -80°C for subsequent use (11123ES60; YEASEN Biotechnology, Shanghai, China). Real-time PCR quantitative analysis was performed using the SYBR Green PCR Kit (11202ES08; YEASEN Biotechnology). Primer sequences are shown in Table 2, and 2<sup>-ΔΔCt</sup> was used for relative quantification of the data.

#### Immunofluorescence

HSC-LX2 cells were seeded in 24-well cell culture plates and treated with relevant reagents for 24 h. Cells were fixed in 4% paraformaldehyde for 15 m, washed with 1× PBS, and blocked with 1% bovine serum albumin for 20 m after reaching the designated treatment time. Cells were incubated with primary antibodies overnight at 4°C and then incubated with fluorescence isothiocyanate-conjugated secondary antibodies for 2 h at room temperature. Cell nuclei were stained with 4',6-diamidino-2-phenylindole (KGA215-50; KeyGen BioTech, Jiangsu, China), and observed and photographed by fluorescence microscopy.

**Table 2. Primer sequences used for qRT-PCR**

ACTA2	F	5'-GCGTGGCTATTCCTTCGTTAC-3'
	R	5'-CATAGTGGTGCCCCCTGATAG-3'
COL1A1	F	5'-ATTCCAGTTCGAGTATGGCGG-3'
	R	5'-GTTGCTTGCTGTTTCCGGGT-3'
FN1	F	5'-AGCCGCCACGTGCCAGGATTAC-3'
	R	5'-CTTATGGGGGTGGCCGTTGTGG-3'
GAPDH	F	5'-CCAACCGCGAGAAGATGA-3'
	R	5'-CCAGAGGCGTACAGGGATAG-3'
ROCK1	F	5'-AGGAAGGCGGACATATTAGTCCCT-3'
	R	5'-AGACGATAGTTGGGTCCCGGC-3'
SLC7A11	F	5'-GGTCCATTACCAGCTTTTGTACG-3'
	R	5'-AATGTAGCGTCCAAATGCCAG-3'

ACAT2, alpha-smooth muscle actin; COL1A1, collagen, type I, alpha 1; FN1, fibronectin-1; ROCK1, Rho-associated protein kinase 1; SLC7A11, solute carrier family 7, member 11.

### **Iron assay**

Iron assay kits (E1042; Applygen Technologies Inc., Beijing, China) were used to determine the relative content of iron in cell lysates.

### **Lipid peroxidation assay**

Lipid peroxidation assay kits (BB4709; BestBio, Shanghai, China) were used to measure the malondialdehyde (MDA) content of cell lysates following the manufacturer's instructions.

### **ROS assay**

Intracellular ROS was assayed with commercial kits (S0033; Beyotime). LX2 cells were seeded in 96-well or 24-well plates and pretreated with relevant reagents for 24 h. A DCFH-DA probe was added to each well, ROS levels were determined 20 m later with a multimode plate reader (EnSpire; PerkinElmer, Waltham, MA, USA) or fluorescence microscopy.

### **GSH assay**

GSH assay kits (BB-4711; BestBio) were used to determine the concentration of reduced GSH following the manufacturer's instructions.

### **Prussian blue staining**

HSC-LX2 cells were seeded in 24-well plates, fixed with 4% paraformaldehyde for 15 m, and stained using a Prussian blue staining kit (G1426; Solarbio Science & Technology Co, Ltd., Beijing, China) following the manufacturer's instructions.

### **Transmission electron microscopy (TEM)**

The morphological characteristics of ferroptosis in HSCs were investigated by TEM. HSC-LX2 cells were seeded in 10-cm culture dishes, transfected with ATF3 siRNA or ROCK1 plasmids for 6 h, treated with Art for 24 h, and in with glutaraldehyde.<sup>24</sup> Images were captured with a Hitachi TEM (HT7700; Tokyo, Japan).

### **Protein stability**

A CHX chase assay was used to determine the stability of ROCK1 protein. Briefly, ROCK1 level was determined by western blotting assay after HSC-LX2 cells were treated with CHX (20  $\mu$ M) for the designated period.

### **Immunoprecipitation**

Immunoprecipitation procedures were performed with Protein A/G Plus MagPoly Beads (RM09008; ABclonal) following the manufacturer's instructions. Bead samples (50  $\mu$ L) were transferred to a 1.5 mL centrifuge tube and placed on a magnetic separator. The protection solution was discarded and 200  $\mu$ L of binding/washing solution was added to the tube and mixed well. The beads were washed twice, 1 mL blocking solution was added and the tubes containing beads were placed on a shaker and incubated on ice for 1 h. The beads were then washed twice with binding/wash solution, bound to the target antibody, reacted on ice for 2 h, added protein samples, and kept on ice overnight on a shaker. After placing the magnetic bead-antigen complex on the magnetic separator, the supernatant was collected for subsequent detection. A 1 mL aliquot of binding/wash solution was added to the tube, mixed by gentle pipetting to perform magnetic separation, the supernatant was discarded and the beads were washed twice. The tubes were removed from the magnetic separator, 60  $\mu$ L 2 $\times$  loading buffer was added and the samples were heated in a water bath at 95°C for 15 m. A mag-

netic separator was to isolate the beads and the supernatant was collected for western blotting.

### **Ubiquitination assay**

The ubiquitin experiment was performed as previously described.<sup>29</sup>

### **JC-1 assay**

JC-1 assay kits (C2003S; Beyotime) were used to measure the mitochondrial membrane potential following the manufacturer's instructions. For staining, 500  $\mu$ L of JC-1 working solution was added to each well of a 24-well plate, diluted 1:200 with staining buffer, and mixed by pipetting several times. The culture media was discarded and adherent cells were washed with PBS and 500  $\mu$ L of new cell culture medium was added to each well together with 500  $\mu$ L of JC-1 staining working solution, mixed, incubated 20 m at 37°C. The supernatant was discarded, the wells were washed twice with JC-1 buffer, 1 mL of new culture media was added, and the results were observed by fluorescence microscopy.

### **Phosphorylated protein assay**

The method was the same as that used for immunoprecipitation. Anti-phospho-SER/THR-PRO MPM-2 was the primary antibody.

### **Calculations and statistics**

The study results were reported as means and standard error of the mean. Student's-*t* tests were used to determine the significance of differences between two groups and one-way analysis of variance and the Student-Newman-Keuls test were used to compare differences among multiple groups. GraphPad Prism version 8 (La Jolla, CA, USA) was used for the statistical analysis. *p*-values<0.05 were considered statistically significant.

## **Results**

### **Art inhibited HSC activation in vitro**

Human activated HSCs, HSC-LX2, were employed in the investigation to examine the efficacy of Art against liver fibrosis *in vitro*. We discovered that Art concentration of 10  $\mu$ M significantly decreased the viability of LX2 cells (Fig. 1A) and was not cytotoxic to LO2 normal human hepatocytes at concentrations of <30  $\mu$ M (Fig. 1B). Hence, LX2 cells were exposed to Art at concentrations of 0, 5, 10, and 20  $\mu$ M in the subsequent experiments. Under these concentrations, we could explore the inhibition of Art on LX2 cells without causing toxic damage to LO2 cells. We noticed that cells formed clusters and cell numbers decreased in a dose-dependent manner (Fig. 1C) and trypan blue staining revealed that the number of dead cells increased as the Art dosage increased (Fig. 1D).

Activated HSCs express a large amount of  $\alpha$ -SMA, transform into myofibroblasts, and synthesize ECM that accumulates in the liver to cause fibrous scarring.<sup>30</sup> Western blotting found that the levels of  $\alpha$ -SMA, Collagen I, and Fibronectin were dose-dependently reduced by Art treatment (Fig. 1E). The RT-PCR and immunofluorescence staining results were similar to those seen in the western blots (Fig. 1 F-I). Our study found that Art inhibited HSC activation by inducing their death.

### **Art inhibited activation of HSC and induced ferroptosis**

Ferroptosis is characterized by the cell membrane rupture

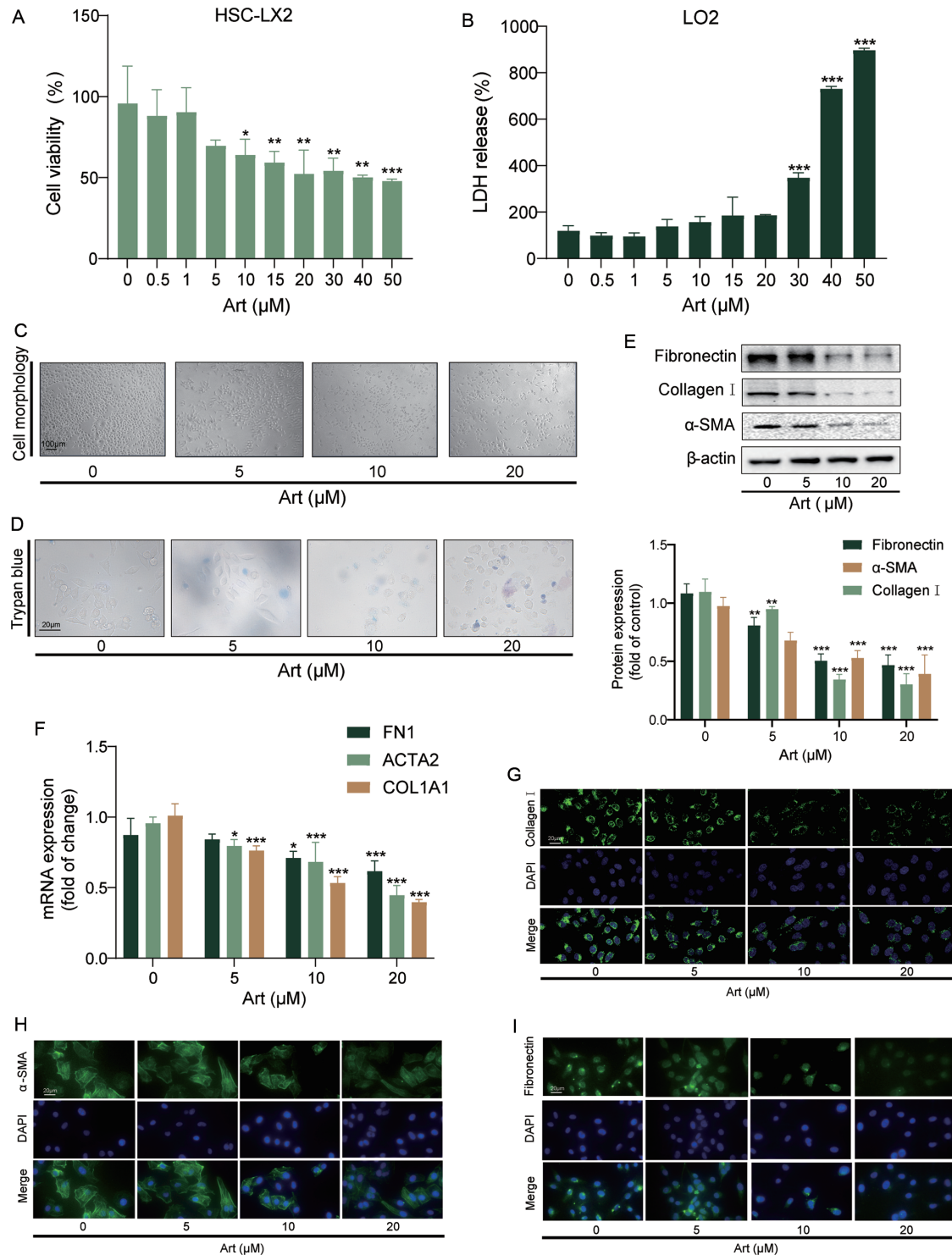


**Fig. 1. Art inhibited HSC activation *in vitro*.** (A) MTT was used to detect the effectiveness of different concentrations of Art on the viability of LX2 cells. The control group was given DMSO in the same volume ( $n \geq 3$  in each group, \* $p < 0.05$ , \*\* $p < 0.01$ , \*\*\* $p < 0.001$ , vs. control group). (B) LDH assay kits were used to determine the toxicity of different concentrations of Art to LO2 cells ( $n \geq 3$  in each group, \* $p < 0.05$ , \*\* $p < 0.01$ , \*\*\* $p < 0.001$ , vs. control group). (C, D) LX2 cells were treated with 5, 10 and 20 μM Art, and the control group was given DMSO in the same volume. Morphological changes of LX2 cells under different drug doses and the number of dead cells stained with trypan blue were observed by electron microscopy. (E) Western blotting was used to detect the protein expression levels of α-SMA, Collagen I and Fibronectin ( $n \geq 3$  in each group, \* $p < 0.05$ , \*\* $p < 0.01$ , \*\*\* $p < 0.001$ , vs. control group). (F) RT-PCR was used to detect the mRNA levels of ACTA2, COL1A1, and FN1 ( $n \geq 3$  in each group, \* $p < 0.05$ , \*\* $p < 0.01$ , \*\*\* $p < 0.001$ , vs. control group). (G-I) Immunofluorescence was used to detect the expression of α-SMA, Collagen I and Fibronectin. MTT, 3-(4,5-Dimethylthiazol-2-yl)-2,5-diphenyltetrazolium bromide; DMSO, dimethyl sulfoxide; LDH, lactate dehydrogenase; Art, artesunate; α-SMA, alpha-smooth muscle actin; RT-PCR, real time polymerase chain reaction; ACTA2, alpha-smooth muscle actin 2; COL1A1, collagen, type I, alpha 1; FN1, fibronectin-1.

as a result of lipid peroxidation. Previous studies have demonstrated that intracellular iron deposition caused excessive ROS and GSH deficiency mediated failure of lipid ROS elimination are listed as its source.<sup>5</sup> Small-molecule ferroptosis inducers, such as erastin, RSL3, and FIN56 have been reported. In addition, some modified artemisinin derivatives, including DHA, artemether (ART), and Art, have been found to promote ferroptosis.<sup>31</sup> We found that Art inhibited liver fibrosis by triggering ferroptosis in LX2 cells. Intracellular ferroptosis is typically measured by the content of the free radical scavenger GSH, Fenton's reagent catalyst iron, the lipid peroxidation product MDA, and intracellular ROS. After Art treatment for 24 h, GSH was significantly reduced and intracellular iron and MDA were significantly increased (Fig. 2A–C). Prussian blue staining revealed that Art increased iron deposition in LX2 cells (Fig. 2D). Meanwhile, we measured intracellular ROS levels in LX2 cells with a live cell workstation, Art increased the intensity of the green fluorescence, indicating a rise in ROS levels (Fig. 2E). JC-1 kit assays revealed decreased red fluorescence intensity and increased green fluorescence intensity in LX2 cells after Art treatment, indicating that the JC-1 dye was converted from a polymer to a monomer and a decrease of mitochondrial membrane potential and mitochondrial dysfunction (Fig. 2F). Morphological changes in Art-treated cells included shrunken mitochondria and indistinct cristae (Fig. 2G). In our investigation, Art caused ferroptosis in LX2 cells in a manner comparable to erastin (10  $\mu$ M), which is a small-molecule ferroptosis inducer that has been shown to block the activity of the SLC7A11/xCT system. Fer-1 effectively removes intracellular ROS and has been acknowledged as a specific ferroptosis inhibitor.<sup>3</sup> We then performed reverse verification using Fer-1 (1  $\mu$ M) and Art (10  $\mu$ M) for subsequent experiments based on our previous research. Unsurprisingly, we discovered that GSH content and mitochondrial membrane potential reduced by Art were reversed after Fer-1 treatment (Fig. 2H, N). Compared with Art administered alone, combined administration of Art and Fer-1 reduced the levels of MDA, ROS, and iron (Fig. 2I–K). Likewise, Western blotting demonstrated that Fer-1 reversed the inhibition of HSC activation indicators by Art (Fig. 2L, M). Our study confirmed that Art had anti-fibrotic activity by inducing ferroptosis in LX2 cells.

#### **Art promoted HSC ferroptosis by increased nuclear accumulation of ATF3 and limiting GSH use**

Antioxidant system inactivation shown SLC7A11 deficiency leads to insufficient intracellular cystine absorption and inadequate GSH synthesis, and ferroptosis in cells.<sup>3</sup> Exogenous of N-acetyl-L-cysteine (NAC) facilitates intracellular GSH synthesis, and GSH increased after the addition of NAC (10 mM) and significantly decreased after Art administration (Fig. 3A). At the same time, NAC drastically inhibited Art-increased intracellular iron, MDA and ROS levels (Fig. 3B–D). Moreover, NAC decreased Art-mediated inhibition of activated HSCs (Fig. 3E). The results confirmed our hypothesis that Art interfered with intracellular GSH homeostasis and induced ferroptosis. Studies have shown that ATF3 inhibits the activity of ferroptosis-related antioxidant systems. SLC7A11 was shown to be the downstream target gene of ATF3.<sup>13,32,33</sup> Is ATF3 related to ferroptosis in LX2 cells caused by Art? To address this question, we constructed an ATF3-overexpression plasmid, which significantly increased expression of ATF3 total protein and nucleoprotein (Fig. 3F and Supplementary Fig. 2C). As expected, ATF3 overexpression substantially reduced SLC7A11 mRNA level (Fig. 3G). Western blots showed that Art increased the expression of ATF3 total protein and nucleoprotein (Fig. 3H and Supplementary Fig. 2A, B). It can

be inferred that Art promoted ferroptosis in LX2 cells because of increased ATF3 nuclear accumulation-mediated GSH-dependent inactivation of antioxidant systems. ATF3 siRNA further verified our hypothesis. The effectiveness of ATF3 siRNA was assessed by western blotting and we selected the first sequence of ATF3 siRNA for subsequent experiments, which also significantly inhibited ATF3 expression in the nucleus (Fig. 3I and Supplementary Fig. 2D). Our results showed that ATF3 interference weakened Art-mediated ferroptosis events including GSH depletion, MDA formation, and iron accumulation in LX2 cells (Fig. 3J–L). In addition, decreased mitochondrial membrane potential recovered after ATF3 interference (Fig. 3M). Intracellular iron deposition was significantly decreased, as revealed by Prussian blue staining (Fig. 3N). ROS probe detection assay showed that Art-induced ROS accumulation recovered after interfering with ATF3 (Fig. 3O). We also observed that aberrant mitochondrial morphology induced by Art was restored by ATF3 interference (Fig. 3P). The results confirmed that ATF3 siRNA reversed the inhibition of the HSC activation markers Fibronectin,  $\alpha$ -SMA, and Collagen I by Art on shown by western blotting (Fig. 3Q). Overall, the results showed that inactivation of the GSH-dependent antioxidant system, which was mediated by ATF3 nuclear accumulation, resulted in the timely failure of ROS removal, which may have resulted in Art-triggered ferroptosis in LX2 cells.

#### **ATF3 nonphosphorylation and nuclear accumulation were regulated by Art-mediated ROCK1 suppression**

ROCK1 and ROCK2 are helically coiled protein kinases and ROCK1 is more enriched in the liver than ROCK2.<sup>34</sup> The ROCK1/2 inhibitor Y27632 has been reported to regulate ATF3 nonphosphorylation and nuclear accumulation in macrophages treated with high-density lipoprotein from systemic lupus erythematosus patients.<sup>21</sup> Nonetheless, the intimate connection between ROCKs and ATF3 needs further investigation. Interestingly, the ROCK1 protein level was significantly reduced after Art treatment compared with ROCK2, which raised the probability that ROCK1 was involved in the regulation of ferroptosis in LX2 cells (Fig. 4A). We constructed a ROCK1 overexpression plasmid to further validate its function in Art-induced ferroptosis (Fig. 4B). Immunoprecipitation experiments demonstrated decreased direct binding of ATF3 and ROCK1 protein with Art treatment (Fig. 4C, D). Furthermore, we discovered a phosphorylation site at amino acid position 162 of the ATF3 polypeptide chain through a qPhos database search. The site may be related to ATF3 nuclear import (Fig. 4E). Currently, there are no commercially available antibodies specific for ATF3 phosphorylation. In this study, we used a phosphorylated antibody that is specific for serine/threonine. Immunoprecipitation experiments found that Art decreased ATF3 phosphorylation that was inhibited by ROCK1 overexpression (Fig. 4F). Immunofluorescence experiments confirmed that plasmid-mediated ROCK1 overexpression reduced Art-induced ATF3 nuclear accumulation (Fig. 4G). Consistent with previous studies, mutation of serine/threonine to glutamate/aspartate maintains constant phosphorylation of the protein, and the mutated protein has slower electrophoretic mobility.<sup>27,28,35</sup> Therefore, we mutated the threonine residues at amino acid 162 of ATF3 polypeptide chain to aspartate to mimic the phosphorylated state. Western blotting found that cellular ATF3 protein had slow electrophoretic mobility when cells were treated with the mutated plasmid, which represented the hyperphosphorylated form of ATF3 (Fig. 4H). As expected, Art induced ATF3 nuclear accumulation, and the ferroptosis phenotype in LX2 cells was reversed by the ATF3 mutant plasmid (Fig. 4I–M).

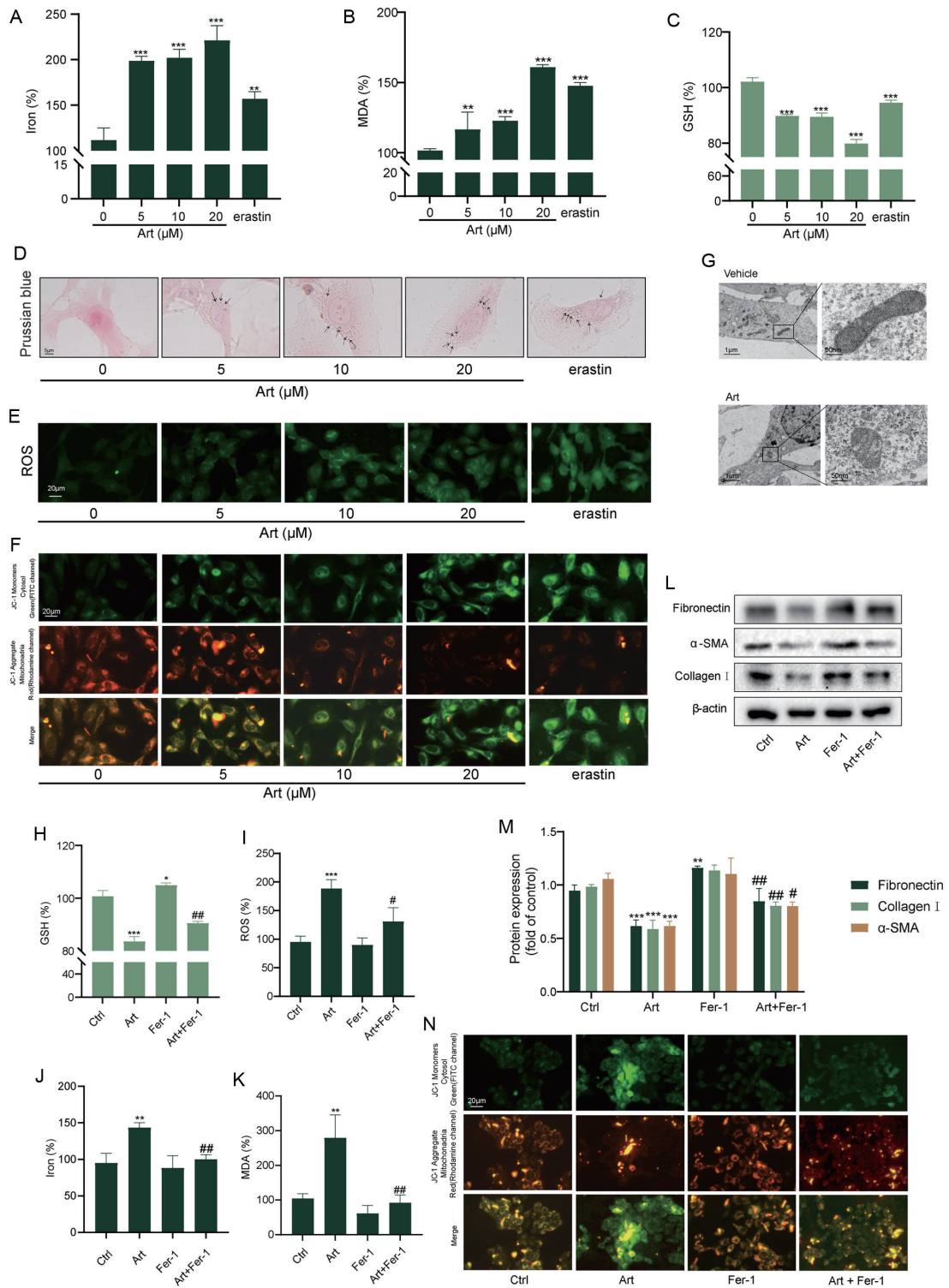


**Fig. 2. Art induced ferroptosis in HSCs and inhibited their activation.** LX2 cells were treated with 5, 10 and 20 μM Art, and the control group was given the same volume of DMSO. The positive control group was given erastin (10 μM) for 24 h ( $n \geq 3$  in each group,  $^*p < 0.05$ ,  $^{**}p < 0.01$ ,  $^{***}p < 0.001$ , vs. control group). (A–C) Assay kits were used to detect the levels of iron, MDA and GSH in LX2 cells. (D) Prussian blue staining was used to detect iron deposition in LX2 cells. (E) A DCFH-DA probe was used to detect ROS content in LX2 cells. (F) JC-1 kits were used to detect the changed membrane potential in LX2 cells. (G) Mitochondrial morphology of LX2 cells was observed by transmission electron microscopy. (H–K) LX2 cells were treated with 1 μM ferrostatin-1 followed by 10 μM Art treatment for 24 h. Kits were employed to detect the levels of iron, MDA, ROS, and GSH in LX2 cells. (L) Western blotting was used to detect the protein expression levels of α-SMA, Collagen I and Fibronectin. (M) It was the quantitative result of Figure L. (N) JC-1 kits were used to detect changes in the mitochondrial membrane potential of LX2 cells treated with Art and then with or without Fer-1 for 24 h. Art, artesunate; MDA, malondialdehyde; GSH, glutathione; ROS, reactive oxygen species; α-SMA, alpha-smooth muscle actin.

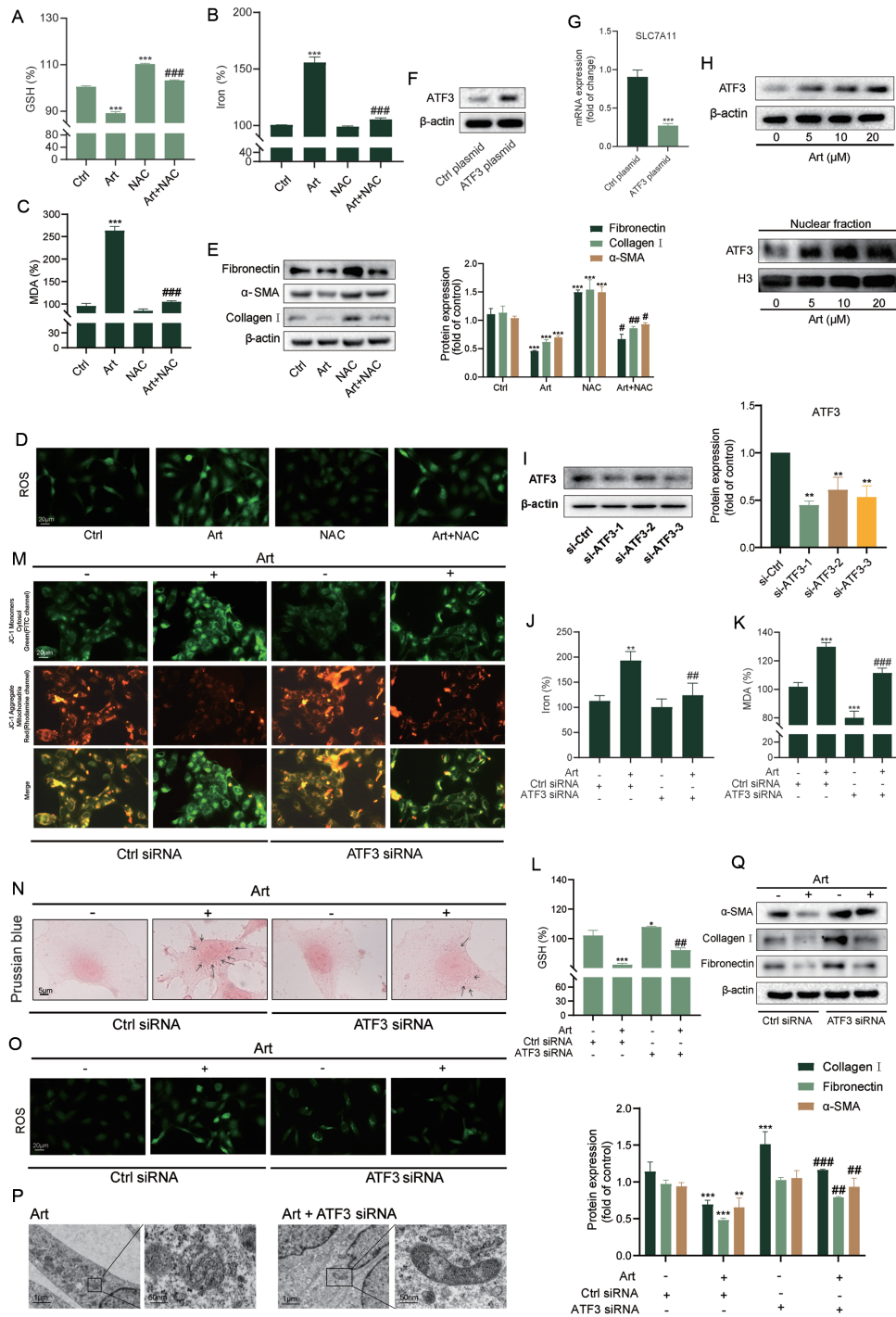


**Fig. 3. Art promoted HSC ferroptosis through nuclear ATF3 upregulation and limiting GSH utilization.** LX2 cells were pretreated with NAC (10 mM) for 1 h, and then Art (10  $\mu$ M) was added and the control group was given DMSO in the same volume for 24 h ( $n \geq 3$  in each group, \* $p < 0.05$ , \*\* $p < 0.01$ , \*\*\* $p < 0.001$ , vs. control group, # $p < 0.05$ , ## $p < 0.01$ , ### $p < 0.001$ , vs. Art group). (A–D) Assay kits were used to detect the GSH, iron, ROS, and MDA in LX2 cells. (E) Western blotting was used to detect  $\alpha$ -SMA, Collagen I and Fibronectin protein expression levels. LX2 cells were transfected with empty vector and ATF3 overexpression plasmid for 6 h. (F) Western blotting was used to verify the transfection efficiency of the ATF3 overexpression plasmid. (G) RT-PCR detected the expression of SLC7A11. LX2 cells were treated with 5, 10, and 20  $\mu$ M Art and the control group was given the same volume of DMSO. (H) Western blotting was used to detect the content of ATF3 in total protein and nucleoprotein. (I) Western blotting to detect the interference effect of ATF3 siRNA. (J–L) LX2 cells were transfected with blank interfering RNA and ATF3 interfering RNA for 6 h, and then treated with Art (10  $\mu$ M) for 24 h. Kits were used to detect the levels of iron, MDA, and GSH in LX2 cells. (M) JC-1 kits were used to detect the change membrane potential in LX2 cells. (N) Prussian blue staining was used to assay iron in LX2 cells. (O) DCFH-DA probes were used to detect the ROS content in LX2 cells. (P) Mitochondrial morphology of LX2 cells was observed by transmission electron microscopy. (Q) Western blotting was used to determine  $\alpha$ -SMA, Collagen I and Fibronectin protein expression levels. NAC, N-acetyl-L-cysteine; GSH, glutathione; ROS, reactive oxygen species; MDA, malondialdehyde; ATF3, activated transcriptional factor 3; RT-PCR, real time polymerase chain reaction; Art, artesunate; DMSO, dimethyl sulfoxide; siRNA, short interfering RNA.

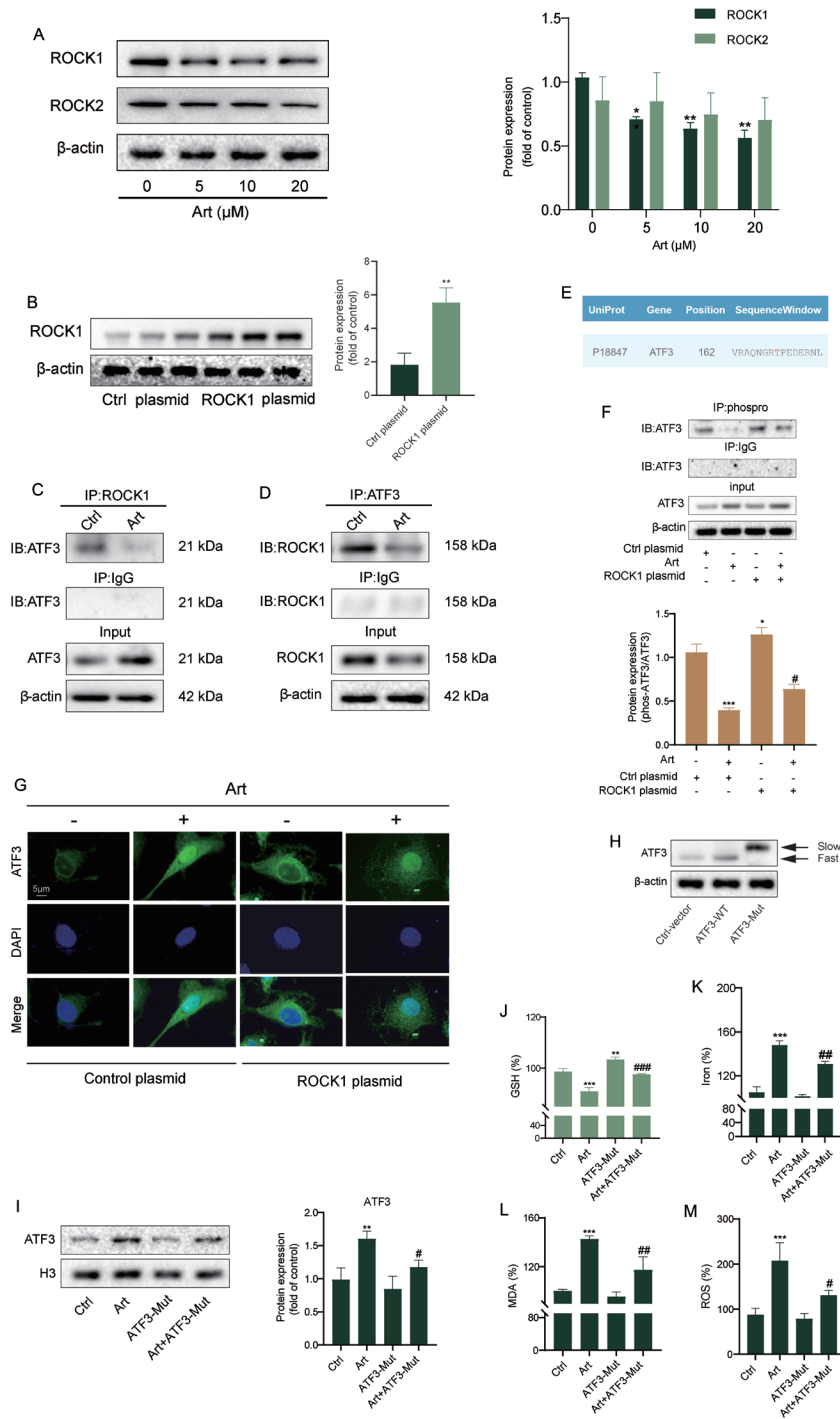


**Fig. 4. Nuclear accumulation of nonphosphorylated ATF3 was regulated by Art-mediated ROCK1 suppression.** LX2 cells were treated with 5, 10, or 20  $\mu$ M Art for 24 h. The control group was given the same volume of DMSO. (A) Western blotting was used to assay the expression of ROCK1 and ROCK2 protein ( $n \geq 3$  in each group,  $^*p < 0.05$ ,  $^{**}p < 0.01$ ,  $^{***}p < 0.001$ , vs. the control group). (B) Western blotting was used to determine the transfection efficiency of the ROCK1 plasmid ( $n \geq 3$  in each group,  $^*p < 0.05$ ,  $^{**}p < 0.01$ ,  $^{***}p < 0.001$ , vs. the control group). (C, D) The binding of ATF3 and ROCK1 was detected by co-immunoprecipitation. (E) Querying ATF3 phosphorylation sites using a Cancerbio database (<http://qphos.cancerbio.info/show.php?type=advanced>). (F) Co-immunoprecipitation was used to detect the phosphorylation of ATF3 ( $n \geq 3$  in each group,  $^*p < 0.05$ ,  $^{**}p < 0.01$ ,  $^{***}p < 0.001$ , vs. control group,  $^{\#}p < 0.05$ ,  $^{\#\#}p < 0.01$ ,  $^{\#\#\#}p < 0.001$ , vs. the Art group). (G) Immunofluorescence was used to detect changes in the nuclear localization of ATF3. LX2 cells transfected with control vector, ATF3-WT, or ATF3-Mut plasmid. (H) Western blotting was used to determine the electrophoretic migration of ATF3 protein. LX2 cells transfected with ATF3-WT or ATF3-Mut plasmid were treated with Art (10  $\mu$ M) for 24 h. (I) Western blotting was used to assay the level of ATF3 in the nucleus. (J–M) Assay kits were used for the detection of GSH, ROS, MDA, and iron level in LX2 cells ( $n \geq 3$  in each group,  $^*p < 0.05$ ,  $^{**}p < 0.01$ ,  $^{***}p < 0.001$ , vs. the control group,  $^{\#}p < 0.05$ ,  $^{\#\#}p < 0.01$ ,  $^{\#\#\#}p < 0.001$ , vs. Art group). Art, artesunate; DMSO, dimethyl sulfoxide; ROCK1, Rho-associated protein kinase 1; ATF3, activated transcriptional factor 3; GSH, glutathione; ROS, reactive oxygen species; MDA, malondialdehyde.

Overall, the results showed that Art regulated ATF3 nuclear accumulation and its function as a TF, relying on inhibition of ROCK1-mediated ATF3 phosphorylation.

#### **Art induced HSC ferroptosis and inhibited HSC activation by promoting ROCK1 ubiquitination**

We observed that Art downregulated ROCK1 protein expression in the previous section (Fig. 4A), thus, we sought to identify the molecular mechanism underlying these changes. A modest increase in ROCK1 mRNA was discovered via RT-PCR, which means that Art-mediated changes in ROCK1 expression might be at the protein rather than the gene level (Fig. 5A). Using the protein synthesis inhibitor-CHX, we proceeded to explore whether the decline in ROCK1 protein was because of decreased synthesis or increased degradation. We examined ROCK1 stability in LX2 cells via CHX treatment with or without Art treatment for 0, 4, 8, or 12 h. We assumed that Art downregulated ROCK1 expression by post-translational modification and promoted protein degradation, as the rate of ROCK1 degradation was significantly enhanced when Art was administered (Fig. 5B–D). Most protein degradation is mediated by autophagy-lysosome and ubiquitin-proteasome procedures, and we primarily explored the impact of these two procedures on ROCK1 degradation. The proteasome inhibitor MG-132 (10  $\mu$ M) and the autophagy inhibitor CQ (20  $\mu$ M) were used to clarify the cause of ROCK1 protein decrease. Our findings demonstrated that Art dramatically decreased ROCK1 expression that was recovered by MG-132 rather than CQ (Fig. 5E, F). In addition, ubiquitination experiments indicated that Art enhanced ROCK1 ubiquitination (Fig. 5G, H). Immediately afterward, we examined ferroptosis indicators changes in the presence of the ROCK1 plasmid, we found that Art-induced ferroptosis in LX2 cells was decreased (Fig. 5K–N). At the same time, mitochondrial shrinkage caused by Art was effectively improved (Fig. 5O). More critically, we examined HSC activation and collagen deposition indexes. These results illustrated that ROCK1 overexpression impaired the inhibitory effectiveness of Art treatment on fibrosis-related markers including Fibronectin, Collagen I and  $\alpha$ -SMA (Fig. 5I, J). Our research revealed that Art stimulated ROCK1 degradation via the ubiquitin-proteasome, thereby reducing its binding to ATF3 and facilitating ATF3 accumulation in the nucleus to induce ferroptosis in LX2 cells.

#### **Art alleviated CCl<sub>4</sub>-induced liver fibrosis in mice**

We demonstrated that ATF3 is critical to anti-liver fibrosis activity of Art *in vitro*. We performed *in vivo* procedures to see whether Art had anti-fibrosis effect consistent with that *in vitro*. It has been reported that HSCs can specifically uptake vitamin A-containing liposomes.<sup>26</sup> VA-Lip-Atf3-shRNA and VA-Lip-Rock1-plasmid constructed with vitamin A-coupled liposomes as carriers specifically altered Atf3 and Rock1 expression of HSCs in the animal model were implemented to verify the contribution of both Atf3 and Rock1 in Art-induced ferroptosis of HSCs *in vivo*. Histological observation indicated that Art decreased the granularity and restored the color of the liver and the orderly arrangement of hepatocytes and decreased continuous vacuoles in the hepatic interstitial space in a dose-dependent manner. HE, Masson, and sirius red staining revealed diminished collagen deposition and hepatic scarring in mice that were intraperitoneally injected with Art at doses of 5 mg/kg and greater (Fig. 6A). The therapeutic effectiveness of Art in CCl<sub>4</sub> model mice were comparable to those of the colchicine group. Serological testing found that Art considerably decreased four liver fibrosis indications [laminin (LN), hyaluronic acid (HA), procollagen type III (PC-

III), IV collagen (IV-C)] and three liver function indicators [aspartate aminotransferase (AST), alanine aminotransferase (ALT), alkaline phosphatase (ALP); Fig. 6B–C]. Immunohistochemistry staining demonstrated that Art greatly suppressed the HSC activation markers,  $\alpha$ -SMA, Collagen I, and Fibronectin, ameliorated the fibrous scarred area in the liver (Fig. 6D). Western blotting revealed that expression of the HSC activation marker,  $\alpha$ -SMA, was considerably decreased by Art treatment (Fig. 6E). Immunofluorescence double-staining indicated that colocalization of EGFR and PDGFR $\beta$  with  $\alpha$ -SMA was reduced in a dose-dependent manner by Art treatment, suggesting that Art was effective in improving collagen deposition in the hepatic vascular region (Fig. 6F, G). Increased iron deposition is an indicator of ferroptosis.<sup>36</sup> Prussian blue staining showed that Art treatment increased iron deposition in the portal region, indicating the occurrence of ferroptosis in HSCs (Fig. 6H).

Further *in vivo* studies found that the HSC-specific Atf3 interference or Rock1 overexpression reduced the effectiveness of Art to improve liver fibrosis, shown by loose arrangement of hepatocytes and increased collagen deposition (Fig. 7A, B). Serological tests showed recovery of three liver function and five liver fibrosis indexes (Fig. 7C, D). Western blotting results revealed that the decrease in the HSC activation index in response to Art was reversed (Fig. 7E). It was assumed that ROCK1 participated in HSC activation, as it was weakly expressed in the normal group and more strongly in the model group.<sup>37</sup> Tissue immunofluorescence showed that the colocalization signal intensity of  $\alpha$ -SMA and ROCK1 in the model group was strong, and that the intensity weakened after Art administration. Moreover, ATF3 expression was greatly increased when Art was given. Either Atf3 deficiency or Rock1 overexpression attenuated the Art-diminished  $\alpha$ -SMA in scar region (Fig. 7F). Prussian blue staining showed that Art-increased iron deposition was attenuated by the interfering plasmid. Furthermore, we isolated primary HSCs from the livers of fibrotic mice for further study. The analysis revealed that the Art-induced ferroptosis phenotype in HSCs was reversed after HSC-specific overexpression of Rock1 or interference with Atf3 (Fig. 7G). The results showed that inhibiting Atf3 or overexpressing Rock1 prevented Art from promoting ferroptosis in activated HSCs.

#### **Discussion**

Currently, no specific therapy has been approved for liver fibrosis. Fortunately, we are aware that scavenging activated HSCs may be a rationale for liver fibrosis medication. Ferroptosis is a recently studied type of programmed cell death that is thought to be involved in the occurrence and development of liver disease.<sup>38–40</sup> Administration of a high-iron diet to liver-specific transferrin knockout mice, made them more susceptible to ferroptosis-induced liver fibrosis.<sup>41</sup> NADPH-cytochrome P450 reductase (POR) and NADH-cytochrome b5 reductase (CYP5R1) knockdown decreased intracellular H<sub>2</sub>O<sub>2</sub> production and decreased lipid peroxidation and ferroptosis. Furthermore, POR knockout in mouse liver reversed concanavalin-induced liver injury.<sup>42</sup> Additionally, our previous study indicated that N<sup>6</sup>-methyladenosine modification activated autophagy and induced ferroptosis in HSCs by maintaining the stability of BECN1 mRNA.<sup>43</sup> Nevertheless, how ferroptosis regulates the occurrence and progression of liver disease needs further exploration.

Artemisinin is a  $\beta$ -sesquiterpene lactone compound with good antimalarial activity. In 1977, Liu *et al*.<sup>44</sup> synthesized Art from artemisinin. Previous studies have shown that the artemisinin derivatives DHA and ART induced ferroptosis in

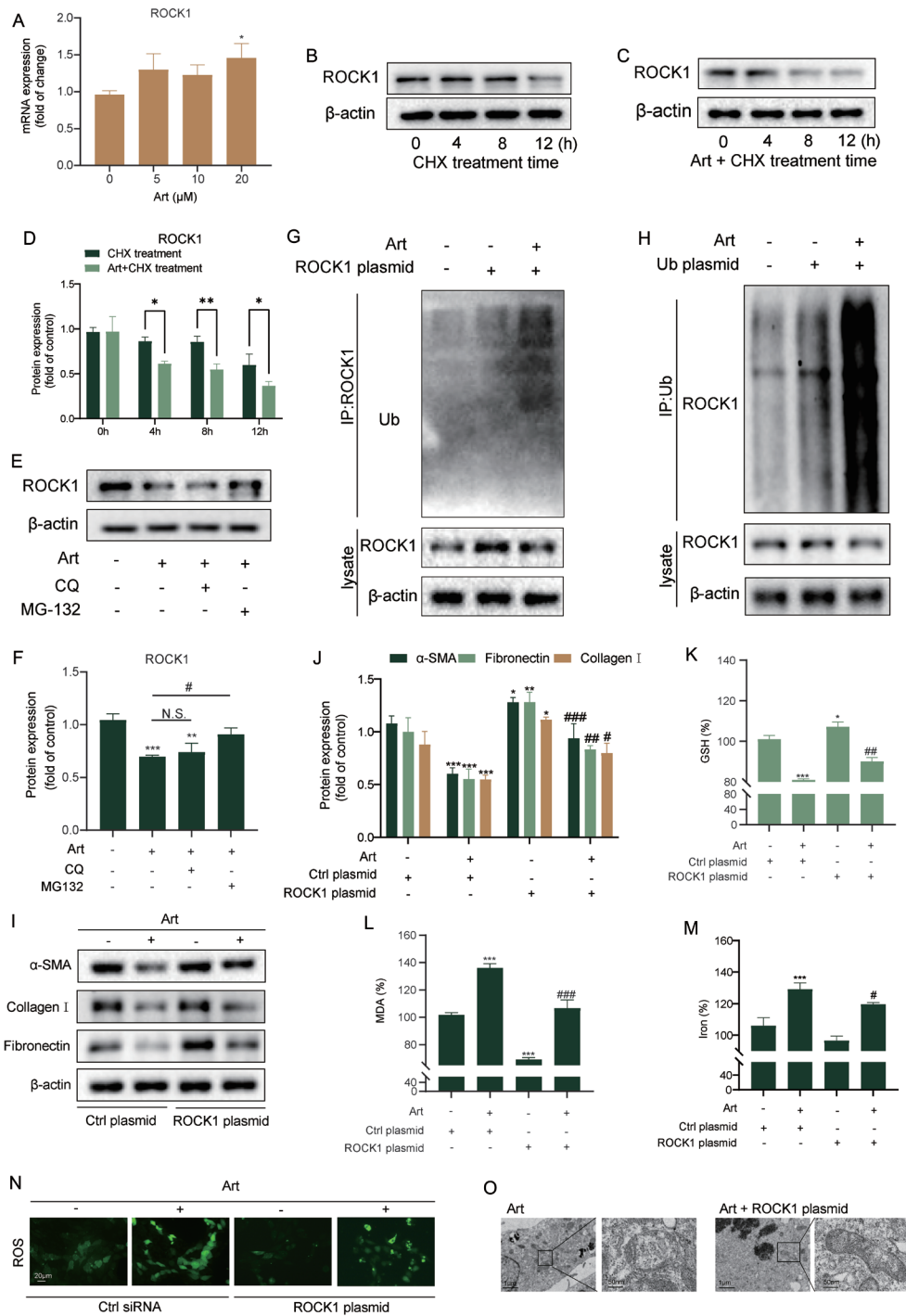


**Fig. 5. Art induced HSCs ferroptosis and inhibited HSCs activation through exacerbating ROCK1 ubiquitination.** (A) mRNA expression of ROCK1 detected by RT-PCR ( $n \geq 3$  in each group,  $*p < 0.05$ , vs. the control group). LX2 cells were treated with 20 μM CHX alone or 10 μM Art and 20 μM CHX for 0, 4, 8, or 12 h. (B, C) Expression of ROCK1 protein was determined by western blotting. (D) Quantification of B and C ( $n \geq 3$  in each group,  $*p < 0.05$ ,  $**p < 0.01$ ). LX2 cells were treated with 10 μM Art alone, 10 μM Art and 10 μM MG-132, or 10 μM Art and 20 μM CQ for 24 h. (E) ROCK1 protein expression was assayed by western blotting. (F) Quantitative results of E. ( $n \geq 3$  in each group,  $*p < 0.05$ ,  $**p < 0.01$ ,  $***p < 0.001$ , vs. the control group, N.S.,  $\#p < 0.05$ ,  $\#\#p < 0.01$ ,  $\#\#\#p < 0.001$ , vs. the Art group). LX2 cells were treated with 10 μM Art followed by HA-Ub or ROCK1 overexpression plasmids. (G, H) ROCK1 ubiquitination was detected by ubiquitination assay. (I, J) Western blotting was used to detect α-SMA, Collagen I, and Fibronectin protein expression levels ( $n \geq 3$  in each group,  $*p < 0.05$ ,  $**p < 0.01$ ,  $***p < 0.001$ , vs. the control group,  $\#p < 0.05$ ,  $\#\#p < 0.01$ ,  $\#\#\#p < 0.001$ , vs. the Art group). LX2 cells were transfected with empty vector or ROCK1 overexpression plasmid for 6 h. (K–N) Assay kits were used to measure GSH, iron, MDA, and ROS levels in LX2 cells ( $n \geq 3$  in each group,  $*p < 0.05$ ,  $**p < 0.01$ ,  $***p < 0.001$ , vs. the control group,  $\#p < 0.05$ ,  $\#\#p < 0.01$ ,  $\#\#\#p < 0.001$ , vs. the Art group). (O) Mitochondrial morphology in LX2 cells was observed by transmission electron microscopy. ROCK1, Rho-associated protein kinase 1; N.S., no significance; RT-PCR, real time polymerase chain reaction; CHX, cycloheximide; Art, artesunate; CQ, chloroquine; α-SMA, alpha-smooth muscle actin; GSH, glutathione; MDA, malondialdehyde; ROS, reactive oxygen species.

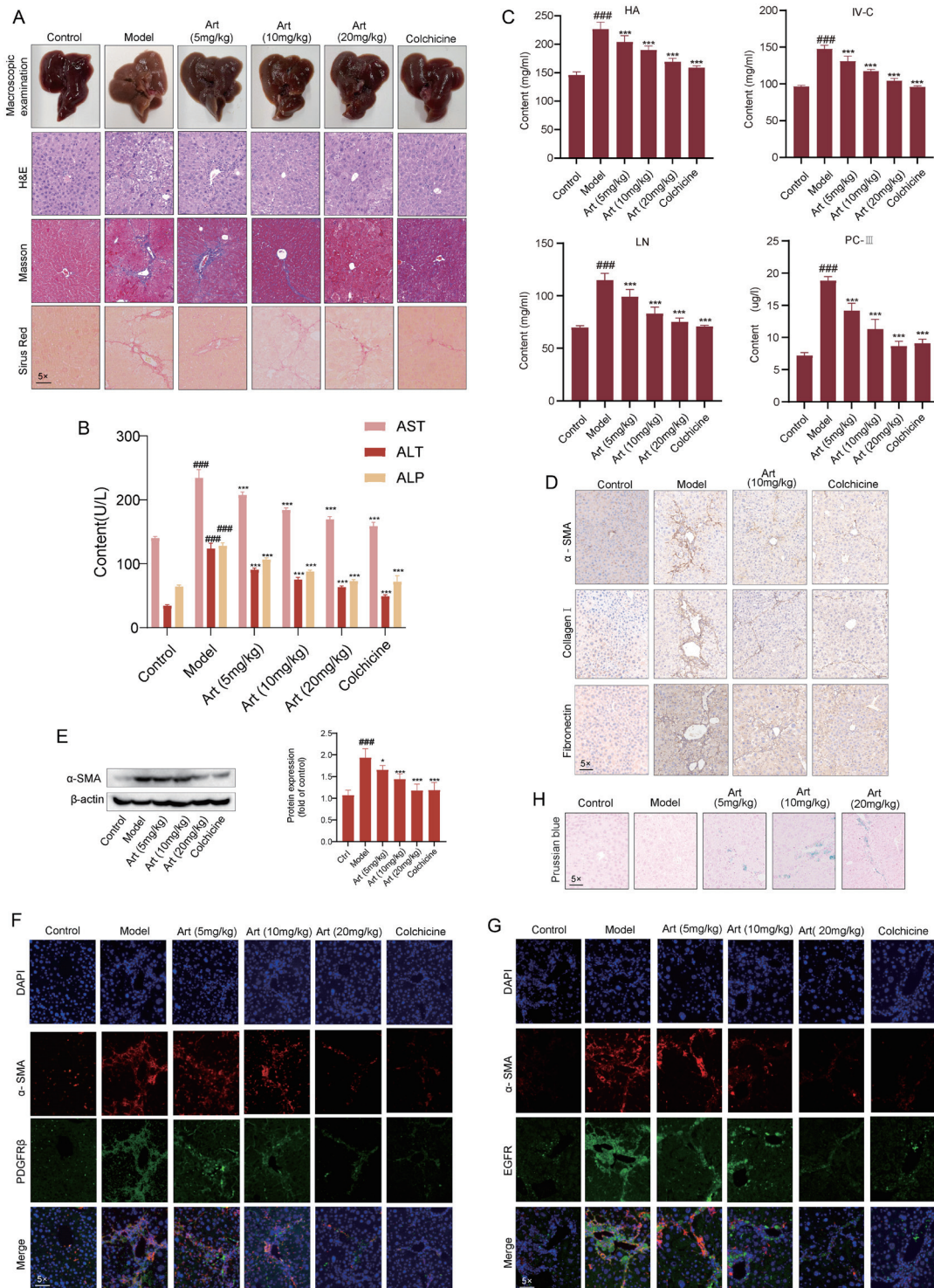


**Fig. 6. Art had a good anti-liver fibrosis effectiveness *in vivo*.** (A) After the animals were killed, the liver was collected and photographed to observe the gross morphology, and liver sections were stained with hematoxylin and eosin, Masson, and sirius red. Representative photographs are shown. (B) ELISA measurement of ALT, AST, and ALP levels in serum ( $n=6$ , in each group,  $^*p<0.05$ ,  $^{**}p<0.01$ ,  $^{***}p<0.001$ , vs. the control group,  $^*p<0.05$ ,  $^{**}p<0.01$ ,  $^{***}p<0.001$ , vs. model group). (C) Levels of LN, HA, PC-III and IV-C measured by ELISA ( $n=6$ , in each group,  $^*p<0.05$ ,  $^{**}p<0.01$ ,  $^{***}p<0.001$ , vs. the control group,  $^*p<0.05$ ,  $^{**}p<0.01$ ,  $^{***}p<0.001$ , vs. the model group). (D) Expression of  $\alpha$ -SMA, Collagen I, and Fibronectin determined by immunohistochemistry. (E) Western blotting of  $\alpha$ -SMA in liver tissue ( $n=6$ , in each group,  $^*p<0.05$ ,  $^{**}p<0.01$ ,  $^{***}p<0.001$ , vs. the control group,  $^*p<0.05$ ,  $^{**}p<0.01$ ,  $^{***}p<0.001$ , vs. the model group). (F-G) Liver sections were subjected to immunofluorescence double-staining using antibodies against PDGFR $\beta$ , EGFR and  $\alpha$ -SMA. (H) Prussian blue staining was used to detect the accumulation of iron in liver tissue. ALT, alanine aminotransferase; AST, aspartate aminotransferase; ALP, alkaline phosphatase; LN, laminin; HA, hyaluronic acid; PC-III, procollagen type III; IV-C, IV collagen;  $\alpha$ -SMA, alpha-smooth muscle actin; PDGFR $\beta$ , platelet-derived growth factor receptor beta; EGFR, epidermal growth factor receptor.

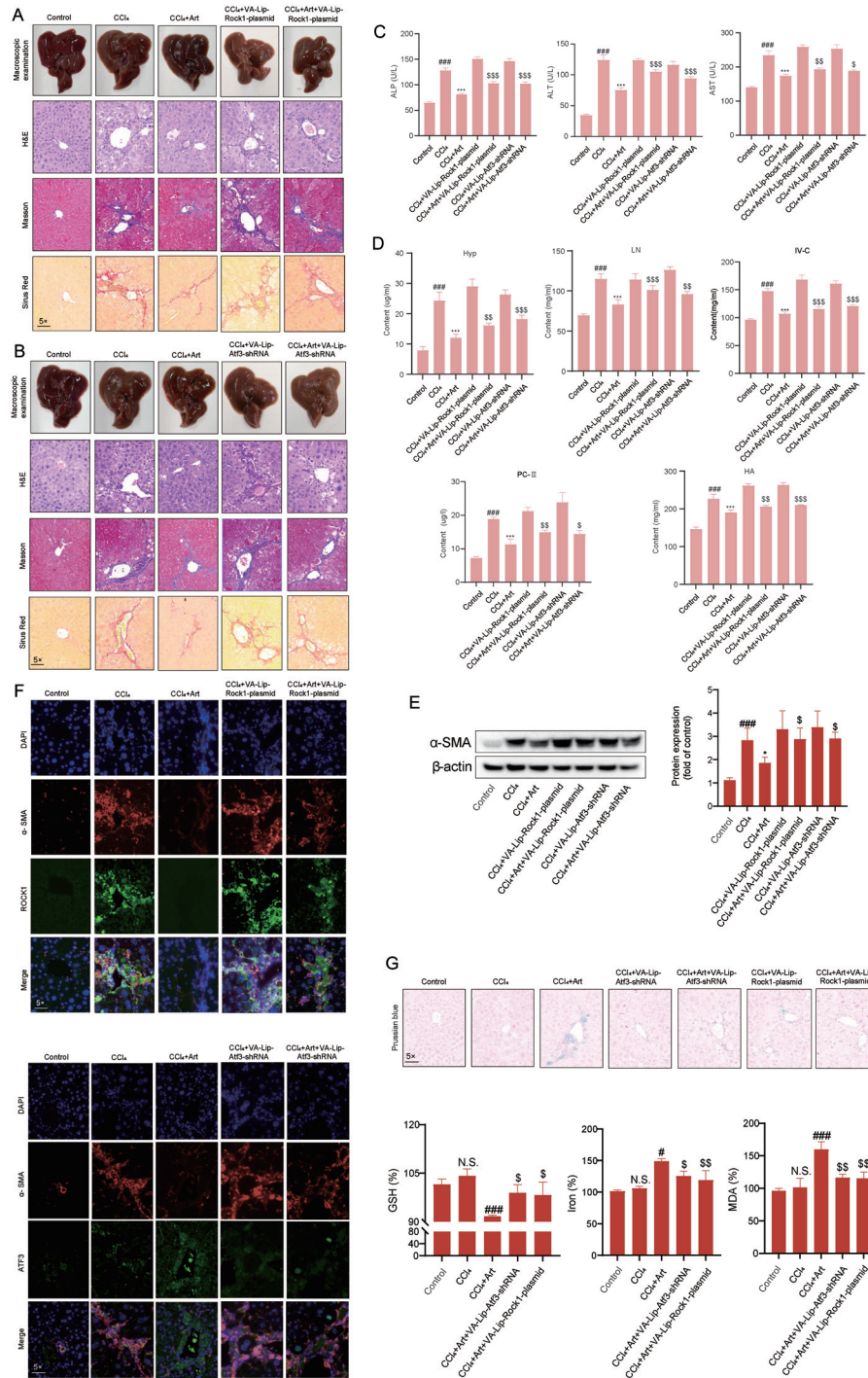


**Fig. 7. Anti-fibrosis effectiveness of Art in mice was decreased by specific interference with Atf3 or overexpressing Rock1.** (A-B) The appearance of livers from each group. (C) ELISA of ALT, AST, and ALP levels in serum ( $n=6$ , in each group,  $^{\#}p<0.05$ ,  $^{\#\#}p<0.01$ ,  $^{\#\#\#}p<0.001$ , vs. the control group,  $^*p<0.05$ ,  $^{**}p<0.01$ ,  $^{***}p<0.001$ , vs. the CCl<sub>4</sub> group,  $^{\$}p<0.05$ ,  $^{\$\$}p<0.01$ ,  $^{\$\$\$}p<0.001$ , vs. the CCl<sub>4</sub> + Art group). (D) ELISA of Hyp, HA, LN, IV-C, and PC-III levels in serum ( $n=6$ , in each group,  $^{\#}p<0.05$ ,  $^{\#\#}p<0.01$ ,  $^{\#\#\#}p<0.001$ , vs. the control group,  $^*p<0.05$ ,  $^{**}p<0.01$ ,  $^{***}p<0.001$ , vs. the CCl<sub>4</sub> group,  $^{\$}p<0.05$ ,  $^{\$\$}p<0.01$ ,  $^{\$\$\$}p<0.001$ , vs. CCl<sub>4</sub>+Art group). (E) Western blotting was used to determine the changes of  $\alpha$ -SMA expression after interference with Atf3 and overexpression of Rock1 ( $n=6$ , in each group,  $^{\#}p<0.05$ ,  $^{\#\#}p<0.01$ ,  $^{\#\#\#}p<0.001$ , vs. the control group,  $^*p<0.05$ ,  $^{**}p<0.01$ ,  $^{***}p<0.001$ , vs. the CCl<sub>4</sub> group,  $^{\$}p<0.05$ ,  $^{\$\$}p<0.01$ ,  $^{\$\$\$}p<0.001$ , vs. CCl<sub>4</sub>+Art group). (F) Immunofluorescence double-staining was used to determine  $\alpha$ -SMA, ROCK1, and ATF3 expression. (G) Prussian blue staining was used to detect liver iron deposition after Atf3 interference and Rock1 overexpression. Assay kits were used to measure GSH, iron, and MDA in primary HSCs after Atf3 interference and Rock1 overexpression ( $n=3$ , in each group, N.S. vs. the control group,  $^{\#}p<0.05$ ,  $^{\#\#}p<0.01$ ,  $^{\#\#\#}p<0.001$ , vs. the CCl<sub>4</sub> group,  $^{\$}p<0.05$ ,  $^{\$\$}p<0.01$ , vs. the CCl<sub>4</sub> + Art group). ALT, alanine aminotransferase; AST, aspartate aminotransferase; ALP, alkaline phosphatase; Hyp, hydroxyproline; HA, hyaluronic acid; LN, laminin; IV-C, IV collagen; PC-III, procollagen type III;  $\alpha$ -SMA, alpha-smooth muscle actin; Atf3, activated transcriptional factor 3; Rock1, Rho-associated protein kinase 1; N.S., no significance; GSH, glutathione; MDA, malondialdehyde; CCl<sub>4</sub>, carbon tetrachloride.

HSCs to produce anti-liver fibrosis activity.<sup>25,45</sup> Similarly, Art may have anti-hepatic fibrosis activity.<sup>23</sup> However, the molecular basis of Art antifibrosis activity need further elucidation, and whether it can be recommended as an anti-hepatic fibrosis medicine needs further pharmacological and toxicological assessment. Our study confirmed that Art inhibited HSC activation *in vitro* and had effective anti-liver fibrosis activity *in vivo*. We also discovered that Art significantly altered the ferroptosis markers in HSCs, among which GSH depletion aroused our curiosity.

Ferroptosis is partially mediated via the inactivation of antioxidative systems including SLC7A11-mediated GSH use, FSP1-mediated CoQ10 activity, and DHODH-mediated CoQH2 pathway.<sup>46,47</sup> SLC7A11 is a cystine-glutamate transporter that provides the raw material for reduced intracellular GSH synthesis that facilitates elimination of intracellular ROS generated when cells experience ferroptosis.<sup>3</sup> Correspondingly, numerous TFs are involved in the regulation of ferroptosis. p53 and NRF2 have been reported to influence ferroptosis by modulating SLC7A11 transcription.<sup>48,49</sup> NRF2 is inactive when binding to KEAP1 in a physiological state. Activated NRF2 binds to ARE on antioxidant genes and initiates their transcription to prevent ferroptosis.<sup>49</sup> p53 suppresses SLC7A11 expression or promotes DPP4 nuclear accumulation, thereby promoting the development of ferroptosis.<sup>50</sup> Moreover, it has been demonstrated that ATF4 activation promotes SLC7A11 expression and induces ferroptosis.<sup>7,51</sup> The results suggest that TFs are extensively implicated in the process of antioxidant system modulation of ferroptosis. The TF ATF3 inhibits SLC7A11 transcriptional activity and it is remarkable that the primary attention on ATF3 is currently on endoplasmic reticulum stress, study of that protein in ferroptosis are still in their infancy.<sup>13,50,52</sup> In this study, we found that Art significantly upregulated nuclear ATF3, which repressed SLC7A11 transcription and promoted ferroptosis in HSCs, and the results warrant further investigation. Modulation of SLC7A11 is not the only way that ATF3 influences ferroptosis. According to a Chip sequencing analysis, ATF3 regulated the transcription of NOX4 and PLA2G6, which are involved in mitochondrial ROS production and scavenging of unsaturated phospholipids.<sup>50</sup> More studies are required to understand how ATF3 manipulates these genes to trigger ferroptosis. Typically, TFs required to be phosphorylated by kinases before they enter the nucleus where they can perform transcriptional regulatory functions. However, certain TFs enter the nucleus without phosphorylation and stay active. For example, the CREB co-activator CRTC is phosphorylated in the basal state interacting with 14-3-3 protein and sequestered in the cytoplasm.<sup>53</sup> Phosphatase PP2A promotes the dephosphorylation of BRZ1 and increases its nuclear accumulation.<sup>54</sup> Upregulated PP2Ac also mediates dephosphorylation and nuclear import of HDAC4 and regulates HMGB1 gene transcription.<sup>55</sup> Comparably, a phosphorylation site, which has been associated with ATF3 intracellular localization, at threonine at position 162 of the ATF3 polypeptide chain has been detected.<sup>21</sup> Phosphorylated ATF3 can be inactive and reside in the cytoplasm and enters the nucleus as nonphosphorylated ATF3 when activated. The ROCK family protein inhibitor Y-27632 boosts ATF3 nuclear accumulation, which might be related to the inhibition of ATF3 phosphorylation in macrophages.<sup>21</sup> Nevertheless, which member of the ROCK family contributes more to the nuclear localization of ATF3 and what is the precise mechanism remains unclear.

ROCK1 is a helical coiled protein kinase and is an essential component of the RhoA/ROCK signaling pathway that promotes the transition of lung fibroblasts to myofibroblasts.<sup>56</sup> PDGF-stimulated HSC undergoes mTOR and ROCK1 activa-

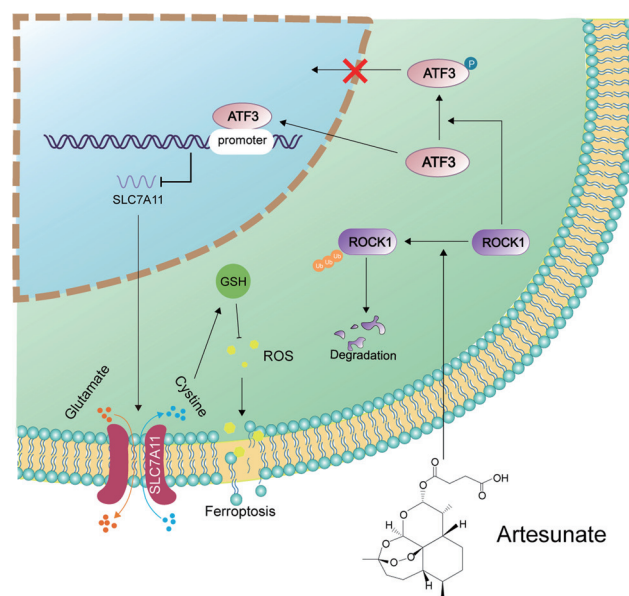


**Fig. 8. Art induced ferroptosis in HSCs by regulating ROCK1 to promote nuclear accumulation of ATF3 and had antifibrosis effectiveness.** Art promotes the degradation of ROCK1 through the ubiquitin-proteasome pathway. It increases the nuclear accumulation of ATF3, inhibits the antioxidant system, especially the activity of SLC7A11, which results in accumulation of ROS in LX2 cells and induces ferroptosis in LX2 cells, and accounts for its anti-liver fibrosis activity. ROCK1, Rho-associated protein kinase 1; ATF3, activated transcription factor 3; SLC7A11, solute carrier family 7, member 11; ROS, reactive oxygen species.

tion, facilitates fibrogenic extracellular vesicles release and promote liver fibrosis.<sup>57</sup> TGF- $\beta$ 1-mediated TGF- $\beta$ 2 activation is dependent on Rho kinase activity, thereby fostering the transition of HSCs to myofibroblasts and liver fibrosis.<sup>58</sup> It has been reported that ROCK1 and EGFR are mainly expressed in hepatocytes.<sup>59,60</sup> Our results found that ROCK1 and EGFR accumulated in the hepatic portal following CCl<sub>4</sub> treatment. The difference may be the result of different causes of liver injury, and the exact reason for this difference needs to be further discussion. However, whether ROCK1 inhibition can slow liver fibrosis progression through ferroptosis pathway requires more investigation. In our study, Art attenuated the direct phosphorylation of ATF3 by ROCK1 and increased ATF3 nuclear accumulation in LX2 cells. Additionally, we observed that Art induce the ubiquitin-proteasomal degradation of ROCK1 while plasmid-mediated ROCK1 redundancy limited Art-induced ferroptosis and attenuated the anti-fibrotic effect of Art (Fig. 8). Our study reported for the first time that Art regulated ferroptosis in HSCs through the ROCK1/ATF3 axis and provided ideas for enriching the network of ferroptosis regulation and indicated that targeted ROCK1/ATF3 axis therapy may be an approach for liver fibrosis medication. It provides a rationale for the study of Art in liver fibrosis treatment.

## Funding

The work was supported by the National Natural Science Foundation of China (No.82000572, 82073914, 82173874, 82274185), the Natural Science Foundation of Jiangsu Province (No.BK20220467, BK20200840), the Major Project of the Natural Science Research of Jiangsu Higher Education Institutions (No.22KJB310013, 19KJA310005), the Joint Project of Jiangsu Key Laboratory for Pharmacology and

Safety Evaluation of Chinese Materia Medica and Yangtze River Pharmaceutical (No.JKLPSE202005), the Natural Science Foundation of Nanjing University of Chinese Medicine (No.NZY82000572), Nanjing Pharmaceutical Association-Changzhou Fourth Pharmaceutical Hospital Pharmaceutical Research Fund (NO.2021YX030), and Postgraduate Research & Practice Innovation Program of Jiangsu Province (No. SJCX22\_0792). Most importantly, I would like to thank my supervisors for their guidance and support for my thesis, my seniors and classmates for their help, my roommates for their patience and understanding, and my family and friends for their unconditional support.

### Conflict of interest

The authors have no conflict of interests related to this publication.

### Author contributions

YW did the experiment, analyzed the data and manuscript writing. YL, YQ, MS, LW, JS, FZ and XX participated in experiments. MG, ZZ and SZ conceived the research idea and designed the study. All authors had access to the study data and approved the final manuscript.

### Ethical statement

The animal experiment procedures were approved by the Institutional and Local Committee on the Care and Use of Animals of Nanjing University of Chinese Medicine, and all animals were given humane care in accordance with the guidelines of the National Institutes of Health (USA).

### Data sharing statement

Data generated or analyzed during this study are available from the corresponding author upon request.

### References

- [1] Englemann C, Claria J, Szabo G, Bosch J, Bernardi M. Pathophysiology of decompensated cirrhosis: Portal hypertension, circulatory dysfunction, inflammation, metabolism and mitochondrial dysfunction. *J Hepatol* 2021;75(Suppl 1):S49–S66. doi:10.1016/j.jhep.2021.01.002, PMID: 34039492.
- [2] Tsuchida T, Friedman SL. Mechanisms of hepatic stellate cell activation. *Nat Rev Gastroenterol Hepatol* 2017;14(7):397–411. doi:10.1038/nrgastro.2017.38, PMID:28487545.
- [3] Dixon SJ, Lemberg KM, Lamprecht MR, Skouta R, Zaitsev EM, Gleason CE, *et al*. Ferroptosis: an iron-dependent form of nonapoptotic cell death. *Cell* 2012;149(5):1060–1072. doi:10.1016/j.cell.2012.03.042, PMID:22632970.
- [4] Zhang Z, Yao Z, Wang L, Ding H, Shao J, Chen A, *et al*. Activation of ferritinophagy is required for the RNA-binding protein ELAVL1/HuR to regulate ferroptosis in hepatic stellate cells. *Autophagy* 2018;14(12):2083–2103. doi:10.1080/15548627.2018.1503146, PMID:30081711.
- [5] Stockwell BR. Ferroptosis turns 10: Emerging mechanisms, physiological functions, and therapeutic applications. *Cell* 2022;185(14):2401–2421. doi:10.1016/j.cell.2022.06.003, PMID:35803244.
- [6] Houesson A, Francois C, Sauzay C, Louandre C, Mongelard G, Godin C, *et al*. Metallothionein-1 as a biomarker of altered redox metabolism in hepatic stellate carcinoma cells exposed to sorafenib. *Mol Cancer* 2016;15(1):38. doi:10.1186/s12943-016-0526-2, PMID:27184800.
- [7] Gao R, Kalathur RKR, Coto-Llerena M, Ercan C, Buechel D, Shuang S, *et al*. YAP/TAZ and ATF4 drive resistance to Sorafenib in hepatocellular carcinoma by preventing ferroptosis. *EMBO Mol Med* 2021;13(12):e14351. doi:10.15252/emmm.202114351, PMID:34664408.
- [8] Tarangelo A, Magtanong L, Biegling-Rolett KT, Li Y, Ye J, Attardi LD, *et al*. p53 Suppresses Metabolic Stress-Induced Ferroptosis in Cancer Cells. *Cell Rep* 2018;22(3):569–575. doi:10.1016/j.celrep.2017.12.077, PMID:29346757.
- [9] Lu F, Lionnet T. Transcription Factor Dynamics. *Cold Spring Harb Perspect Biol* 2021;13(11):a040949. doi:10.1101/cshperspect.a040949, PMID:34001530.
- [10] Chen H, Pugh BF. What do Transcription Factors Interact With? *J Mol Biol*

- 2021;433(14):166883. doi:10.1016/j.jmb.2021.166883, PMID:33621520.
- [11] Zhou H, Li N, Yuan Y, Jin YG, Guo H, Deng W, *et al*. Activating transcription factor 3 in cardiovascular diseases: a potential therapeutic target. *Basic Res Cardiol* 2018;113(5):37. doi:10.1007/s00395-018-0698-6, PMID:30094473.
- [12] Lu S, Wang XZ, He C, Wang L, Liang SP, Wang CC, *et al*. ATF3 contributes to brucine-triggered glioma cell ferroptosis via promotion of hydrogen peroxide and iron. *Acta Pharmacol Sin* 2021;42(10):1690–1702. doi:10.1038/s41401-021-00700-w, PMID:34112960.
- [13] Wang L, Liu Y, Du T, Yang H, Lei L, Guo M, *et al*. ATF3 promotes erastin-induced ferroptosis by suppressing system Xc(.). *Cell Death Differ* 2020;27(2):662–675. doi:10.1038/s41418-019-0380-z, PMID:31273299.
- [14] Li Y, Li Z, Zhang C, Li P, Wu Y, Wang C, *et al*. Cardiac Fibroblast-Specific Activating Transcription Factor 3 Protects Against Heart Failure by Suppressing MAP2K3-p38 Signaling. *Circulation* 2017;135(21):2041–2057. doi:10.1161/CIRCULATIONAHA.116.024599, PMID:28249877.
- [15] Zhang J, Wang H, Chen H, Li H, Xu P, Liu B, *et al*. ATF3-activated accelerating effect of LINC00941/lncIAPF on fibroblast-to-myofibroblast differentiation by blocking autophagy depending on ELAVL1/HuR in pulmonary fibrosis. *Autophagy* 2022;18(11):2636–2655. doi:10.1080/15548627.2022.2046448, PMID:35427207.
- [16] Xu Y, Hu S, Jadhav K, Zhu Y, Pan X, Bawa FC, *et al*. Hepatocytic Activating Transcription Factor 3 Protects Against Steatohepatitis via Hepatocyte Nuclear Factor 4alpha. *Diabetes* 2021;70(11):2506–2517. doi:10.2337/db21-0181, PMID:34475098.
- [17] Li GB, Cheng Q, Liu L, Zhou T, Shan CY, Hu XY, *et al*. Mitochondrial translocation of cofilin is required for allyl isothiocyanate-mediated cell death via ROCK1/PTEN/PI3K signaling pathway. *Cell Commun Signal* 2013;11:50. doi:10.1186/1478-811X-11-50, PMID:23895248.
- [18] Wang QL, Xing W, Yu C, Gao M, Deng LT. ROCK1 regulates sepsis-induced acute kidney injury via TLR2-mediated endoplasmic reticulum stress/pyroptosis axis. *Mol Immunol* 2021;138:99–109. doi:10.1016/j.molimm.2021.07.022, PMID:34365196.
- [19] Peng L, Sang H, Wei S, Li Y, Jin D, Zhu X, *et al*. circCUL2 regulates gastric cancer malignant transformation and cisplatin resistance by modulating autophagy activation via miR-142-3p/ROCK2. *Mol Cancer* 2020;19(1):156. doi:10.1186/s12943-020-01270-x, PMID:33153478.
- [20] Sawada N, Liao JK. Rho/Rho-associated coiled-coil forming kinase pathway as therapeutic targets for statins in atherosclerosis. *Antioxid Redox Signal* 2014;20(8):1251–1267. doi:10.1089/ars.2013.5524, PMID:23919640.
- [21] Smith CK, Seto NL, Vivekanandan-Giri A, Yuan W, Playford MP, Manna Z, *et al*. Lupus high-density lipoprotein induces proinflammatory responses in macrophages by binding lectin-like oxidized low-density lipoprotein receptor 1 and failing to promote activating transcription factor 3 activity. *Ann Rheum Dis* 2017;76(3):602–611. doi:10.1136/annrheumdis-2016-209683, PMID:27543414.
- [22] Augustin Y, Staines HM, Krishna S. Artemisinins as a novel anti-cancer therapy: Targeting a global cancer pandemic through drug repurposing. *Pharmacol Ther* 2020;216:107706. doi:10.1016/j.pharmthera.2020.107706, PMID:33075360.
- [23] Kong Z, Liu R, Cheng Y. Artesunate alleviates liver fibrosis by regulating ferroptosis signaling pathway. *Biomed Pharmacother* 2019;109:2043–2053. doi:10.1016/j.biopha.2018.11.030, PMID:30551460.
- [24] Zhang Z, Guo M, Li Y, Shen M, Kong D, Shao J, *et al*. RNA-binding protein ZFP36/TTP protects against ferroptosis by regulating autophagy signaling pathway in hepatic stellate cells. *Autophagy* 2020;16(8):1482–1505. doi:10.1080/15548627.2019.1687985, PMID:31679460.
- [25] Shen M, Guo M, Li Y, Wang Y, Qiu Y, Shao J, *et al*. m(6A) methylation is required for dihydroartemisinin to alleviate liver fibrosis by inducing ferroptosis in hepatic stellate cells. *Free Radic Biol Med* 2022;182:246–259. doi:10.1016/j.freeradbiomed.2022.02.028, PMID:35248719.
- [26] Sato Y, Murase K, Kato J, Kobune M, Sato T, Kawano Y, *et al*. Resolution of liver cirrhosis using vitamin A-coupled liposomes to deliver siRNA against a collagen-specific chaperone. *Nat Biotechnol* 2008;26(4):431–442. doi:10.1038/nbt1396, PMID:18376398.
- [27] Ren QN, Zhang H, Sun CY, Zhou YF, Yang XF, Long JW, *et al*. Phosphorylation of androgen receptor by mTORC1 promotes liver steatosis and tumorigenesis. *Hepatology* 2022;75(5):1123–1138. doi:10.1002/hep.32120, PMID:34435708.
- [28] Wang Q, Barshop WD, Bian M, Vashisht AA, He R, Yu X, *et al*. The Blue Light-Dependent Phosphorylation of the CCE Domain Determines the Photosensitivity of Arabidopsis CRY2. *Mol Plant* 2017;10(2):357. doi:10.1016/j.molp.2016.12.009, PMID:28196586.
- [29] Su Y, Zhao D, Jin C, Li Z, Sun S, Xia S, *et al*. Dihydroartemisinin Induces Ferroptosis in HCC by Promoting the Formation of PEBP1/15-LO. *Oxid Med Cell Longev* 2021;2021:3456725. doi:10.1155/2021/3456725, PMID:34925691.
- [30] Bourebaba N, Marycz K. Hepatic stellate cells role in the course of metabolic disorders development - A molecular overview. *Pharmacol Res* 2021;170:105739. doi:10.1016/j.phrs.2021.105739, PMID:34171492.
- [31] Chen GQ, Benthani FA, Wu J, Liang D, Bian ZX, Jiang X. Artemisinin compounds sensitize cancer cells to ferroptosis by regulating iron homeostasis. *Cell Death Differ* 2020;27(1):242–254. doi:10.1038/s41418-019-0352-3, PMID:31114026.
- [32] Lu Z, McBrearty N, Chen J, Tomar VS, Zhang H, De Rosa G, *et al*. ATF3 and CH25H regulate effector trogocytosis and anti-tumor activities of endogenous and immunotherapeutic cytotoxic T lymphocytes. *Cell Metab* 2022;34(9):1342–1358.e1347. doi:10.1016/j.cmet.2022.08.007, PMID:3607682.
- [33] He L, Feng A, Guo H, Huang H, Deng Q, Zhao E, *et al*. LRG1 mediated by ATF3 promotes growth and angiogenesis of gastric cancer by regulat-

- ing the SRC/STAT3/VEGFA pathway. *Gastric Cancer* 2022;25(3):527–541. doi:10.1007/s10120-022-01279-9, PMID:35094168.
- [34] Riento K, Ridley AJ. Rocks: multifunctional kinases in cell behaviour. *Nat Rev Mol Cell Biol* 2003;4(6):446–456. doi:10.1038/nrm1128, PMID:12778124.
- [35] Rozansky DJ, Cornwall T, Subramanya AR, Rogers S, Yang YF, David LL, *et al*. Aldosterone mediates activation of the thiazide-sensitive Na-Cl cotransporter through an SGK1 and WNK4 signaling pathway. *J Clin Invest* 2009;119(9):2601–2612. doi:10.1172/JCI38323, PMID:19690383.
- [36] Wu K, Fei L, Wang X, Lei Y, Yu L, Xu W, *et al*. ZIP14 is involved in iron deposition and triggers ferroptosis in diabetic nephropathy. *Metallomics* 2022;14(7):mfac034. doi:10.1093/mtomcs/mfac034, PMID:35641158.
- [37] Huang C, Gan D, Luo F, Wan S, Chen J, Wang A, *et al*. Interaction Mechanisms Between the NOX4/ROS and RhoA/ROCK1 Signaling Pathways as New Anti-fibrosis Targets of Ursolic Acid in Hepatic Stellate Cells. *Front Pharmacol* 2019;10:431. doi:10.3389/fphar.2019.00431, PMID:31130857.
- [38] Hassannia B, Vandenabeele P, Vanden Berghe T. Targeting Ferroptosis to Iron Out Cancer. *Cancer Cell* 2019;35(6):830–849. doi:10.1016/j.ccell.2019.04.002, PMID:31105042.
- [39] Lei P, Ayton S, Bush AI. The essential elements of Alzheimer's disease. *The Journal of Biological Chemistry* 2021;296:100105. doi:10.1074/jbc.REV120.008207, PMID:33219130.
- [40] Fang X, Ardehali H, Min J, Wang F. The molecular and metabolic landscape of iron and ferroptosis in cardiovascular disease. *Nat Rev Cardiol* 2023;20(1):7–23. doi:10.1038/s41569-022-00735-4, PMID:35788564.
- [41] Yu Y, Jiang L, Wang H, Shen Z, Cheng Q, Zhang P, *et al*. Hepatic transferrin plays a role in systemic iron homeostasis and liver ferroptosis. *Blood* 2020;136(6):726–739. doi:10.1182/blood.2019002907, PMID:32374849.
- [42] Yan B, Ai Y, Sun Q, Ma Y, Cao Y, Wang J, *et al*. Membrane Damage during Ferroptosis Is Caused by Oxidation of Phospholipids Catalyzed by the Oxidoreductases POR and CYB5R1. *Mol Cell* 2021;81(2):355–369.e310. doi:10.1016/j.molcel.2020.11.024, PMID:33321093.
- [43] Shen M, Li Y, Wang Y, Shao J, Zhang F, Yin G, *et al*. N(6)-methyladenosine modification regulates ferroptosis through autophagy signaling pathway in hepatic stellate cells. *Redox Biol* 2021;47:102151. doi:10.1016/j.redox.2021.102151, PMID:34607160.
- [44] Efferth T, Dunstan H, Sauerbrey A, Miyachi H, Chitambar CR. The anti-malarial artesunate is also active against cancer. *Int J Oncol* 2001;18(4):767–773. doi:10.3892/ijo.18.4.767, PMID:11251172.
- [45] Li Y, Jin C, Shen M, Wang Z, Tan S, Chen A, *et al*. Iron regulatory protein 2 is required for artemether -mediated anti-hepatic fibrosis through ferroptosis pathway. *Free Radic Biol Med* 2020;160:845–859. doi:10.1016/j.freeradbiomed.2020.09.008, PMID:32947011.
- [46] Bersuker K, Hendricks JM, Li Z, Magtanong L, Ford B, Tang PH, *et al*. The CuQ oxidoreductase FSP1 acts parallel to GPX4 to inhibit ferroptosis. *Nature* 2019;575(7784):688–692. doi:10.1038/s41586-019-1705-2, PMID:31634900.
- [47] Mao C, Liu X, Zhang Y, Lei G, Yan Y, Lee H, *et al*. DHODH-mediated ferroptosis defence is a targetable vulnerability in cancer. *Nature* 2021;593(7860):586–590. doi:10.1038/s41586-021-03539-7, PMID:33981038.
- [48] Kang R, Kroemer G, Tang D. The tumor suppressor protein p53 and the ferroptosis network. *Free Radic Biol Med* 2019;133:162–168. doi:10.1016/j.freeradbiomed.2018.05.074, PMID:29800655.
- [49] Fan Z, Wirth AK, Chen D, Wruck CJ, Rauh M, Buchfelder M, *et al*. Nrf2-Keap1 pathway promotes cell proliferation and diminishes ferroptosis. *Oncogenesis* 2017;6(8):e371. doi:10.1038/oncsis.2017.65, PMID:28805788.
- [50] Liu Z, Gu S, Lu T, Wu K, Li L, Dong C, *et al*. IFI6 depletion inhibits esophageal squamous cell carcinoma progression through reactive oxygen species accumulation via mitochondrial dysfunction and endoplasmic reticulum stress. *J Exp Clin Cancer Res* 2020;39(1):144. doi:10.1186/s13046-020-01646-3, PMID:32727517.
- [51] Zhu S, Zhang Q, Sun X, Zeh HJ 3rd, Lotze MT, Kang R, *et al*. HSPA5 Regulates Ferroptotic Cell Death in Cancer Cells. *Cancer Res* 2017;77(8):2064–2077. doi:10.1158/0008-5472.CAN-16-1979, PMID:28130223.
- [52] Isaac R, Goldstein I, Furth N, Zilber N, Streim S, Boura-Halfon S, *et al*. TM7SF3, a novel p53-regulated homeostatic factor, attenuates cellular stress and the subsequent induction of the unfolded protein response. *Cell Death Differ* 2017;24(1):132–143. doi:10.1038/cdd.2016.108, PMID:27740623.
- [53] Altarejos JY, Montminy M. CREB and the CREC co-activators: sensors for hormonal and metabolic signals. *Nat Rev Mol Cell Biol* 2011;12(3):141–151. doi:10.1038/nrm3072, PMID:21346730.
- [54] Xiong M, Yu JW, Wang JD, Gao Q, Huang LC, Chen C, *et al*. Brassinosteroids regulate rice seed germination through the BZR1-RAMY3D transcriptional module. *Plant Physiol* 2022;189(1):402–418. doi:10.1093/plphys/kiac043, PMID:35139229.
- [55] Lin TB, Hsieh MC, Lai CY, Cheng JK, Wang HH, Chau YP, *et al*. Melatonin relieves neuropathic allodynia through spinal MT2-enhanced PP2Ac and downstream HDAC4 shuttling-dependent epigenetic modification of hmgbl1 transcription. *J Pineal Res* 2016;60(3):263–276. doi:10.1111/jpi.12307, PMID:26732138.
- [56] Datta A, Sandilands E, Mostov KE, Bryant DM. Fibroblast-derived HGF drives acinar lung cancer cell polarization through integrin-dependent RhoA-ROCK1 inhibition. *Cell Signal* 2017;40:91–98. doi:10.1016/j.celsig.2017.09.001, PMID:28888686.
- [57] Gao J, Wei B, de Assuncao TM, Liu Z, Hu X, Ibrahim S, *et al*. Hepatic stellate cell autophagy inhibits extracellular vesicle release to attenuate liver fibrosis. *J Hepatol* 2020;73(5):1144–1154. doi:10.1016/j.jhep.2020.04.044, PMID:32389810.
- [58] Shimada H, Staten NR, Rajagopalan LE. TGF-beta1 mediated activation of Rho kinase induces TGF-beta2 and endothelin-1 expression in human hepatic stellate cells. *J Hepatol* 2011;54(3):521–528. doi:10.1016/j.jhep.2010.07.026, PMID:21087804.
- [59] Wang D, Xu H, Fan L, Ruan W, Song Q, Diao H, *et al*. Hyperphosphorylation of EGFR/ERK signaling facilitates long-term arsenite-induced hepatocytes epithelial-mesenchymal transition and liver fibrosis in sprague-dawley rats. *Ecotoxicol Environ Saf* 2023;249:114386. doi:10.1016/j.ecoenv.2022.114386, PMID:36508792.
- [60] Tak J, Kim YS, Kim TH, Park GC, Hwang S, Kim SG. Galph(12) overexpression in hepatocytes by ER stress exacerbates acute liver injury via ROCK1-mediated miR-15a and ALOX12 dysregulation. *Theranostics* 2022;12(4):1570–1588. doi:10.7150/thno.67722, PMID:35198058.